
Large-Scale Actionless Video Pre-Training via Discrete Diffusion for Efficient Policy Learning

Haoran He^{1,2} Chenjia Bai² Ling Pan¹ Weinan Zhang³ Bin Zhao^{2,4} Xuelong Li^{2,5}

Abstract

Learning a generalist embodied agent capable of completing multiple tasks poses challenges, primarily stemming from the scarcity of action-labeled robotic datasets. In contrast, a vast amount of human videos exist, capturing intricate tasks and interactions with the physical world. Promising prospects arise for utilizing actionless human videos for pre-training and transferring the knowledge to facilitate robot policy learning through limited robot demonstrations. In this paper, we introduce a novel framework that leverages a unified discrete diffusion to combine generative pre-training on human videos and policy fine-tuning on a small number of action-labeled robot videos. We start by compressing both human and robot videos into unified video tokens. In the pre-training stage, we employ a discrete diffusion model with a mask-and-replace diffusion strategy to predict future video tokens in the latent space. In the fine-tuning stage, we harness the imagined future videos to guide low-level action learning trained on a limited set of robot data. Experiments demonstrate that our method generates high-fidelity future videos for planning and enhances the fine-tuned policies compared to previous state-of-the-art approaches with superior generalization ability.

1. Introduction

How do we derive a general-purpose robot agent that can complete a wide variety of tasks? We believe that recent advances in vision and language give us a clue, which delves into pre-training foundation models on extremely large and diverse datasets, followed by fine-tuning on specific do-

main. For instance, through pre-training on internet-scale datasets (Penedo et al., 2023), large language models (Touvron et al., 2023a;b; OpenAI et al., 2023) and vision models (Blattmann et al., 2023; Ramesh et al., 2022; Saharia et al., 2022) showcase impressive performance on various downstream tasks such as question answering, coding, and image generation. However, in contrast to general visual language tasks that can exploit copious amounts of data available on the Internet, embodied tasks necessitate high-quality egocentric data in robotics domains for precise control. Collecting such data can be expensive or time-consuming due to the reliance on robot interactions through teleoperation or kinematic solvers (Hansen et al., 2022). While recent efforts (Bharadhwaj et al., 2023b; Walke et al., 2023a;b; Collaboration, 2023) aim to provide a collection of robot data to cover a wide range of environments and tasks, significant gaps in embodiments and dynamics persist when applying them to specific robot tasks. In contrast to the limited availability of robot data, there is a wealth of human interaction videos capturing intricate tasks and varied interactions with the physical world (Grauman et al., 2022). These videos inherently encapsulate rich semantic information regarding objects, environmental backgrounds, and hand-object interactions across diverse scenarios, making them potentially valuable for acquiring shareable knowledge relevant to embodied tasks.

Motivated by this, existing methods learn image representations pre-trained on human data via temporal contrastive (Nair et al., 2022; Ma et al., 2023b) or patch inpainting (Radosavovic et al., 2022; Xiao et al., 2022), while they focus on visual complexity rather than behavior learning of human activities. Other works try to understand human behaviors by learning reward functions via video-language correspondence (Chen et al., 2021a; Ma et al., 2023a) or extracting hand trajectories as plans for transferring to robots (Bahl et al., 2022; Wang et al., 2023a; Shaw et al., 2022). Nevertheless, it either requires handling the domain gaps between humans and robots or necessitates precise tracking of human hands. Recent attempts train a world model (Hafner et al., 2020; 2021) on human videos and fine-tune the model on robot data (Mendonca et al., 2023; Wu et al., 2023), while they focus on step-by-step transition modeling rather than the long-term behaviors. To effectively utilize

¹Hong Kong University of Science and Technology ²Shanghai Artificial Intelligence Laboratory ³Shanghai Jiao Tong University ⁴Northwestern Polytechnical University ⁵Institute of Artificial Intelligence (TeleAI), China Telecom Corp Ltd. Correspondence to: Chenjia Bai <baichenjia@pjlab.org.cn>.

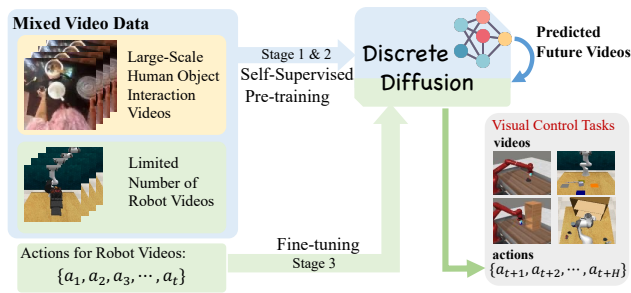


Figure 1. Overall framework of our methods. The video tokens are pre-trained on a mixed dataset of human and robot data. Then the discrete diffusion model is trained on video tokens from the mixed dataset for video prediction. The action-labeled robot data is finally used to fine-tune the diffusion model for generative planning, assisted by the predicted videos in the previous stage.

actionless human videos for embodied agents with a limited amount of action-labeled robot data, we identify three key desiderata for effective pre-training and transfer: (i) an **unified visual representation** for both human and robot data, reducing the domain gaps between them; (ii) **video-level modeling** instead of image-level representations to capture behavior patterns for planning in embodied tasks; (iii) a **scalable architecture for actionless and action-labeled data**, facilitating extensive domain-generic pre-training using videos alone and domain-specific policy learning with videos and actions.

To satisfy all three criteria, we propose a **Video-based Policy learning framework via Discrete Diffusion (VPDD)**. VPDD bridges the visual gap between the human and robot domains by training on the latent space learned from a Vector-Quantized Variational Auto-Encoder (VQ-VAE) (van den Oord et al., 2017). By leveraging large-scale human-robot mixed data for pre-training, we employ video prediction to acquire the commonsense knowledge shared between human and robot interactions. In contrast to existing methods that pre-train image representations, video prediction captures the underlying temporal dynamics essential for long-term planning, which also enhances the policy fine-tuning with foresight from future video predictions. To tackle the challenge of modeling the noisy and multimodal distribution of videos while enabling the simultaneous generation of both videos and actions, we leverage the generative capability and flexible architecture offered by discrete diffusion models (Austin et al., 2023; Gu et al., 2022). Specifically, we formulate both video prediction and action learning as denoising problems within a unified discrete diffusion process (Hu et al., 2023). During the fine-tuning stage, the diffusion model leads to the capability of simultaneously generating the two-domain sequences (i.e., videos and actions) for both video prediction and generative planning (Zhang et al., 2022), which forms a policy implicitly. An overview of our method is given in Figure 1.

In summary, our proposed VPDD framework consists of three stages. (i) Learning compressed video tokens of both human and robot videos by employing a VQ-VAE. (ii) In the pre-training stage with actionless videos, the action tokens are masked and the diffusion model is trained to forecast video tokens in the latent space with a mask-and-replace diffusion strategy. The raw videos can be reconstructed using the codebook learned by VQ-VAE. (iii) In the fine-tuning stage with action-labeled robot videos, the diffusion model learns to simultaneously predict future video tokens and action tokens within the trajectory. This stage leverages extensive knowledge gained through human video prediction, concentrating on training parameters specifically associated with action tokens.

We conduct thorough experiments using human videos from Ego4D (Grauman et al., 2022), as well as embodied datasets from Meta-World (Yu et al., 2020) and RL Bench (James et al., 2020), showcasing its ability to predict high-fidelity future videos. Furthermore, the action-prediction policy also exhibits superior performance compared to previous state-of-the-art approaches (He et al., 2023; Nair et al., 2022; Goyal et al., 2023; Shridhar et al., 2022; Chen et al., 2021b), encompassing both seen and unseen scenes. Videos and codes are provided at <https://video-diff.github.io>.

2. Preliminaries

2.1. Multi-Task POMDP

In this work, we consider a generalist vision-based agent that is capable of addressing multi-task predicaments, where the landscape is characterized by the inherent challenge of acquiring different skills across tasks and partial observability when dealing with image inputs. Given a specific task $\mathcal{T} \sim p(\mathcal{T})$, we further approach the problem as a task-specified Partially Observable Markov Decision Process (POMDP), defined as $(\mathcal{S}^{\mathcal{T}}, \mathcal{O}, \mathcal{A}, \mathcal{P}^{\mathcal{T}}, \mathcal{R}^{\mathcal{T}}, \mu^{\mathcal{T}}, \gamma)$. Here, \mathcal{O} is a shared observation space as we use image observations for all tasks. We also assume all tasks share the same action space with the same embodiment.

2.2. Vector Quantized Model

In order to unify the feature space of both human videos and robot videos, we leverage the Vector Quantized Variational Auto Encoder (VQ-VAE) (van den Oord et al., 2017) to compress high-dimensional data points into information-rich discretized latent codes. Given a high-dimensional video segment $\mathbf{x} \in \mathbb{R}^{T \times H \times W \times C}$, the encoder E first converts it to the temporal-spatial features $\mathbf{z} = E(\mathbf{x}) = \{z_{m,i,l}\} \in \mathbb{R}^{t \times h \times w \times d}$, where $t \times h \times w$ represents the encoded sequence length and is much smaller than $T \times H \times W$. Then we transfer the continuous features into discrete space by performing a nearest neighbors lookup in a codebook of

embeddings $\mathcal{Z} = \{e_j\}_{j=1}^J \in \mathbb{R}^{J \times d}$ to obtain the tokens

$$z_q = \text{Quantize}(z_{m,i,l}) := \arg \min_J \|z_{m,i,l} - e_j\|_2^2, \quad (1)$$

where the video tokens $z_q \in \mathbb{R}^{t \times h \times w \times d}$ can be faithfully reconstructed via a decoder, i.e., $\hat{x} = G(z_q)$. The encoder E , decoder G , and codebook \mathcal{Z} can be trained end-to-end via the following loss function $\mathcal{L} = \|\mathbf{x} - \hat{\mathbf{x}}\|_1 + \|\text{sg}[E(\mathbf{x})] - z_q\|_2^2 + \beta \|\text{sg}[z_q] - E(\mathbf{x})\|_2^2$, where sg denotes stop gradient.

2.3. Discrete Diffusion Model

The discrete diffusion model was first proposed to deal with discrete state space with transitions converging to a binomial distribution (Sohl-Dickstein et al., 2015), and then extended to multinomial diffusion with more options for transition matrices (Hoogeboom et al., 2021; Austin et al., 2023). In this work, we utilize discrete diffusion with the absorbing state for sequence prediction of discrete tokens. Besides J tokens from a codebook, an additional [MASK] token is introduced. We denote \mathbf{x}_k as a one-hot vector identifying the token index. The forward process from \mathbf{x}_{k-1} to \mathbf{x}_k follows a Categorical distribution of $\mathbf{Q}_k \mathbf{x}_{k-1}$, as

$$q(\mathbf{x}_k | \mathbf{x}_{k-1}) = \text{Cat}(\mathbf{x}_k; p = \mathbf{Q}_k \mathbf{x}_{k-1}) = \mathbf{x}_k^T \mathbf{Q}_k \mathbf{x}_{k-1}, \quad (2)$$

where $[\mathbf{Q}_k]_{m,n} = q(\mathbf{x}_k = m | \mathbf{x}_{k-1} = n) \in \mathbb{R}^{(J+1) \times (J+1)}$ is the Markov transition matrix from $k-1$ to k , which is formulated as:

$$\mathbf{Q}_{k-1 \rightarrow k} = \begin{pmatrix} \alpha_k + \beta_k & \beta_k & \beta_k & \cdots & 0 \\ \beta_k & \alpha_k + \beta_k & \beta_k & \cdots & 0 \\ \beta_k & \beta_k & \alpha_k + \beta_k & \cdots & 0 \\ \vdots & \vdots & \vdots & \ddots & \vdots \\ \gamma_k & \gamma_k & \gamma_k & \cdots & 1 \end{pmatrix}, \quad (3)$$

where $\alpha_k \in [0, 1]$ is the probability of retaining the token, and each ordinary token has a probability of γ_k to be replaced by [MASK] token, leaving a chance of $\beta_k = (1 - \alpha_k - \gamma_k)/J$ to be diffused. Importantly, due to the property of the Markov chain, we can derive the probability of \mathbf{x}_k at arbitrary timestep directly from \mathbf{x}_0 as

$$q(\mathbf{x}_k | \mathbf{x}_0) = \mathbf{x}_k^T \bar{\mathbf{Q}}_k \mathbf{x}_0, \text{ with } \bar{\mathbf{Q}}_k = \mathbf{Q}_k \cdots \mathbf{Q}_1. \quad (4)$$

Besides, the posterior of this diffusion process is tractable as $q(\mathbf{x}_{k-1} | \mathbf{x}_k, \mathbf{x}_0) = \frac{q(\mathbf{x}_k | \mathbf{x}_{k-1}, \mathbf{x}_0) q(\mathbf{x}_{k-1} | \mathbf{x}_0)}{q(\mathbf{x}_k | \mathbf{x}_0)} = \frac{(\mathbf{x}_k^T \mathbf{Q}_k \mathbf{x}_{k-1})(\mathbf{x}_{k-1}^T \bar{\mathbf{Q}}_{k-1} \mathbf{x}_0)}{\mathbf{x}_k^T \bar{\mathbf{Q}}_k \mathbf{x}_0}$. In the reverse process, rather than explicitly predicting the posterior through a denoising neural network, the \mathbf{x}_0 -parameterisation enhances stability and allows for fast inference (by skipping Δk steps per iteration). The reverse transition with reparameterisation is formulated as

$$p_\theta(\mathbf{x}_{k-1} | \mathbf{x}_k) = \sum_{\tilde{\mathbf{x}}_0} q(\mathbf{x}_{k-1} | \mathbf{x}_k, \tilde{\mathbf{x}}_0) p_\theta(\tilde{\mathbf{x}}_0 | \mathbf{x}_k), \quad (5)$$

where the neural network predicts the logits of the target data $q(\mathbf{x}_0)$.

3. Methodology

We commence with the pre-training of our model through future video prediction, enabling the learning of a general dynamic pattern across diverse domains. Subsequently, we fine-tune the model using a limited dataset of robot data for policy learning, leveraging foresight from predicted videos. Our framework is illustrated in Figure 2.

3.1. Data Preparing and Tokenizing

Robot Data Collection. We use the rule-based script policy to rollout 20 expert demonstrations for each task in Meta-World (Yu et al., 2020). We also run VPDD on 16 tasks from RL Bench (James et al., 2020), a more challenging benchmark involving 6-Dof manipulation that necessitates multi-view images from a 3D scene to select actions. Following the multi-view manipulation frameworks (Goyal et al., 2023; Shridhar et al., 2022), we utilize the script motion-planner to collect 10 demonstrations for each task. Each demonstration from robot-data is formulated as $\tau_i = \{v_1, a_1, \dots, v_t, a_t, \dots, v_T, a_T\}$ with $v_t = [o_{t-I+1}, \dots, o_{t-1}, o_t]$, where we set $I = 4$ throughout the paper and a denotes the actions. In the context of Meta-World, o_t represents a single-view RGB image at timestep t . For RL Bench, $o_t = \{o_t^{\text{front}}, o_t^{\text{left}}, o_t^{\text{right}}, o_t^{\text{wrist}}\}$ comprises 4 RGB multi-view images (i.e., front, left shoulder, right shoulder, and wrist). Consequently, in RL Bench, v_t is formulated as $v_t = \{v_t^{\text{front}}, v_t^{\text{left}}, v_t^{\text{right}}, v_t^{\text{wrist}}\}$.

Human Data Collection. As for human data collection, we obtain untrimmed videos from the open-sourced Ego4D dataset (Grauman et al., 2022), which contains massive-scale human-object interactions of various durations ranging from 5 seconds to 7 hours. Similar to the data preprocessing in Mu et al. (2023), we filter out videos without human-object interaction and segment each video into short clips with 8-frame intervals. Thus each video is represented as $\tau_i = \{v_1, v_2, \dots, v_n\}$, where v_t denotes a clip containing 4 frames. This approach yields a total of 996,177 clips of human videos, comprising approximately 4M frames. More details on data collection and processing are given in §C.1.

VQ-VAE Encoding. To extract useful features from raw videos in both human and robot domains, a conventional approach is to directly encode them into an embedding space using pre-trained vision models like ViT. However, these models are usually specifically trained on image dataset (Russakovsky et al., 2014), posing a significant challenge due to the domain gap with our interaction videos. Thus, we leverage VQ-VAE to compress the diverse and noisy videos into discrete latent codes, which provide a unified codebook for mixed videos and alleviate the domain gaps between human and robot videos. Formally, we adopt the VQ-VAE architecture introduced by Yan et al. (2021) for encoding videos into a discrete latent space. The codebook

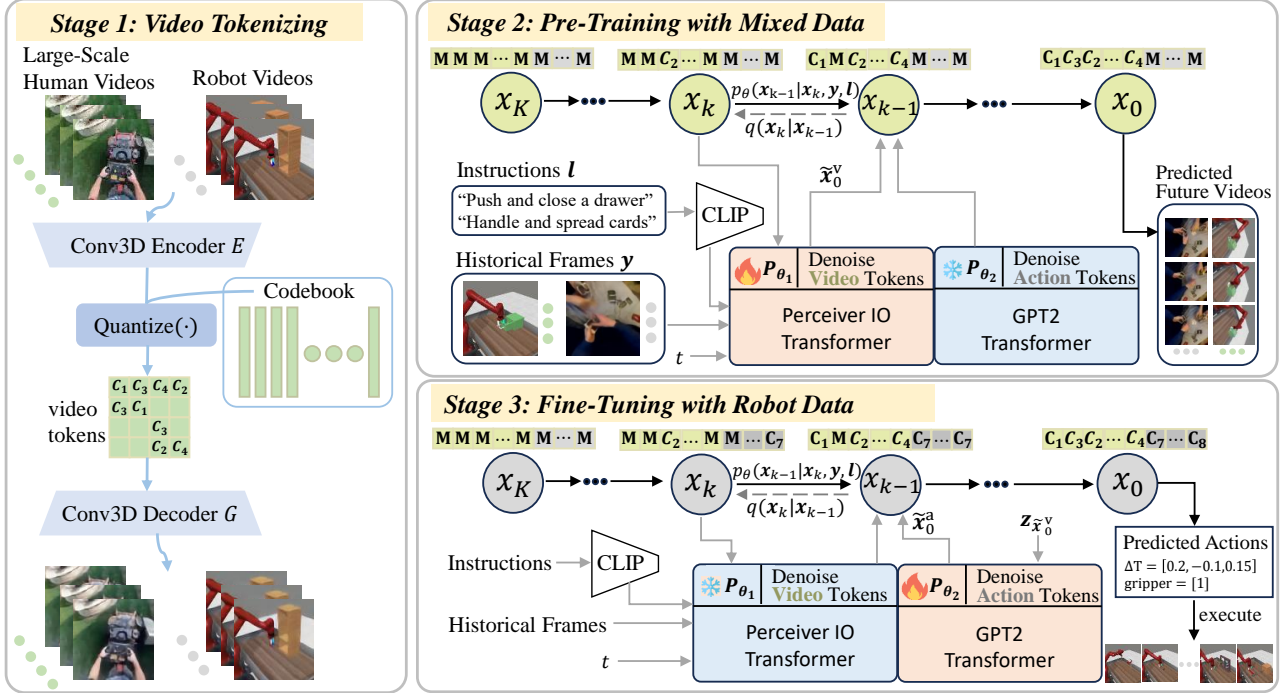


Figure 2. **Overall pipeline of VPDD.** A video-based VQ-VAE is leveraged to encode both human and robot videos into discrete latent codes. Subsequently, a unified discrete diffusion is firstly pre-trained on these video latent codes via a self-supervised objective, predicting future videos conditioning on language instructions and historical videos. The pre-trained video prediction model p_{θ_1} can capture temporal dynamics and task-specific representations. Lastly, we fine-tune our diffusion model on a limited number of robot data. In each diffusion step of the fine-tuning stage, we leverage p_{θ_1} to provide hidden representations $z_{\tilde{x}_0^v}$ to accelerate downstream action learning with video foresight. This integration of video prediction and action learning is achieved through our unified discrete diffusion.

comprises 2048 codes, each represented by 256-dimensional embeddings. The encoder architecture consists of a series of 3D convolutions that downsample by a factor of 4 over space-time (resulting in a $64 \times$ total reduction), followed by 6 attention residual blocks. Consequently, each video clip $v_t \in \{\tau_i\}$ is embedded into latent codes e_t . The architecture for the decoder is the reverse of the encoder, featuring attention residual blocks followed by an equivalent number of 3D transposed convolutions for upsampling over space-time. The VQ-VAE is pre-trained on large-scale videos and remains fixed in the subsequent processes, providing flexibility for various downstream utilization methods.

Action Discretizing. For subsequent pre-training and fine-tuning, we process the collected continuous actions via uniform action discretization (Janner et al., 2021; Brohan et al., 2023). In the case of Meta-World, the action space is a 2-tuple consisting of the change in the 3D space of the end-effector followed by a normalized torque that the gripper fingers should apply. Here all the continuous dimensions are discretized into 48 bins uniformly. Thus, the robot action can be represented using ordinals of the discrete bins as a 4 integer number. For RL Bench, an action consists of the gripper open state and 6-DoF pose including position

and rotation. The position is discretized into 360 bins, and rotation is discretized into Euler angles as 1-degree bins for each of the 3 rotation axes (Shridhar et al., 2022). Gripper open state is a binary value.

3.2. Video Prediction via Unified Discrete Diffusion

Extracting general patterns useful for downstream decision-making from large-scale in-the-wild human videos is challenging, primarily because of the absence of labeled actions and the complexity of the underlying structure of human interactions. Different from previous ways of learning a visual representation, we propose a novel objective to further unleash the representation and temporal modeling ability of diffusion models. Specifically, after obtaining discrete tokens from VQ-VAE encoding, we train a unified discrete diffusion model on the latent space via a self-supervised objective. This objective involves predicting future videos based on observed historical videos for both humans and robots, while masking action tokens. Benefiting from the proposed objective and the x_0 -parameterisation of discrete diffusion, the diffusion model is incentivized to capture both the high-level temporal dynamics and the low-level visual commonalities between historical and future videos

at each diffusion step. Then the acquired knowledge can be leveraged to guide action denoising at each step.

Unified Transition Matrix. The presence of a transition matrix determines the nature of the discrete diffusion model (Austin et al., 2023). While the original discrete diffusion is limited to one modality, drawing inspiration from UniD3 (Hu et al., 2023), which enhances the transition matrix to encompass both images and text, we construct a unified transition matrix to capture global connections between the two modalities—videos and actions. The matrix $[\mathbf{Q}_k]_{m,n}$ below illustrates the unified transition process:

$$\mathbf{Q}_k = \begin{array}{c} \left[\begin{array}{cccc|cccc} \alpha_k + \beta_k & \beta_k & \cdots & \beta_k & 0 & 0 & \cdots & 0 \\ \beta_k & \alpha_k + \beta_k & \cdots & \beta_k & 0 & 0 & \cdots & 0 \\ \vdots & \vdots & \ddots & \vdots & \vdots & \vdots & \ddots & \vdots \\ \beta_k & \beta_k & \cdots & \alpha_k + \beta_k & 0 & 0 & \cdots & 0 \end{array} \right] \\ \left[\begin{array}{cccc|cccc} 0 & 0 & \cdots & 0 & \alpha_k + \beta_k^* & \beta_k^* & \cdots & \beta_k^* \\ 0 & 0 & \cdots & 0 & \beta_k^* & \alpha_k + \beta_k^* & \cdots & \beta_k^* \\ \vdots & \vdots & \ddots & \vdots & \vdots & \vdots & \ddots & \vdots \\ 0 & 0 & \cdots & 0 & \beta_k^* & \beta_k^* & \cdots & \alpha_k + \beta_k^* \end{array} \right] \\ \left[\begin{array}{cccc|cccc} \gamma_k & \gamma_k & \cdots & \gamma_k & \gamma_k & \gamma_k & \cdots & \gamma_k \end{array} \right] \end{array} \quad \left. \begin{array}{l} 0 \\ 0 \\ \vdots \\ 0 \\ 0 \\ 0 \\ \vdots \\ 0 \\ 1 \end{array} \right\}$$

where β_k and β_k^* are the probabilities of a token to be replaced by any other accessible tokens in different modalities. The dimension of \mathbf{Q}_k is $(J + J^* + 1) \times (J + J^* + 1)$, where J and J^* are the number of tokens in different modalities, i.e., J is the size of codebook in VQ-VAE and J^* is the number of action classes in discretization. The sum of each column in this transition matrix is one to preserve probability mass. Mathematically, we have $\beta_k = (1 - \alpha_k - \gamma_k)/J$ and $\beta_k^* = (1 - \alpha_k - \gamma_k)/J^*$. All the mass of the stationary distribution falls on the [MASK] token, which satisfies the prerequisite for a discrete diffusion model transition matrix (Austin et al., 2023). The details of the diffusion process are provided in §A.1.

Unified Objective. We cast both video prediction and action learning as a conditional generative problem, and the goal is to maximize $\mathbb{E}_{\tau \sim \cup_i \tau_i} [\log p_{\theta}(\mathbf{x}_0(\tau) | \mathbf{y}(\tau), \mathbf{l})]$. Here $\mathbf{x} = [\mathbf{x}^v, \mathbf{x}^a]$, where $\mathbf{x}^v = [e_{t+h+1}, \dots, e_{t+h+M}]$ represents future video segments with M clips, and $\mathbf{x}^a = [a_t, \dots, a_{t+H-1}]$ denotes action sequences of H steps. $\mathbf{y} = e_t$ serves as the condition containing historical video tokens. \mathbf{l} is the language instructions describing current tasks. In practice, we train two separate denoising networks, namely $p_{\theta_1}(\mathbf{x}_{k-1}^v | \mathbf{x}_k, \mathbf{y}, \mathbf{l})$ and $p_{\theta_2}(\mathbf{x}_{k-1}^a | \mathbf{x}_k, z_{\tilde{\mathbf{x}}_0^v}, \mathbf{l})$, to learn videos and actions, respectively. Here, $z_{\tilde{\mathbf{x}}_0^v}$ represents the hidden representation of predicted future videos given by p_{θ_1} at each diffusion step, which is utilized to guide action learning. Formally, $\tilde{\mathbf{x}}_0^v = \text{Softmax}(\text{MLP}(z_{\tilde{\mathbf{x}}_0^v}))$. As the actions are absent during the pre-training stage, we mask \mathbf{x}^a and freeze p_{θ_2} , as illustrated in Figure 2. The network is trained to minimize the following variational lower bound (VLB) (Sohl-Dickstein et al., 2015; Gu et al., 2022):

$$\mathcal{L}_{\text{vlb}} = \mathcal{L}_0 + \sum_{k=2}^K \mathcal{L}_{k-1} + \mathcal{L}_K, \quad (6)$$

where

$$\begin{aligned} \mathcal{L}_0 &= -\mathbb{E}_{q(\mathbf{x}_1 | \mathbf{x}_0)} [\log p_{\theta_1}(\mathbf{x}_0^v | \mathbf{x}_1, \mathbf{y}, \mathbf{l}) + \log p_{\theta_2}(\mathbf{x}_0^a | \mathbf{x}_1, z_{\tilde{\mathbf{x}}_0^v}, \mathbf{l})], \\ \mathcal{L}_{k-1} &= \mathbb{E}_{q(\mathbf{x}_k | \mathbf{x}_0)} [D_{\text{KL}}(q(\mathbf{x}_{k-1} | \mathbf{x}_k, \mathbf{x}_0) \\ &\quad \| [p_{\theta_1}(\mathbf{x}_{k-1}^v | \mathbf{x}_k, \mathbf{y}, \mathbf{l}); p_{\theta_2}(\mathbf{x}_{k-1}^a | \mathbf{x}_k, z_{\tilde{\mathbf{x}}_0^v}, \mathbf{l})])], \\ \mathcal{L}_K &= \mathbb{E}_{q(\mathbf{x}_0)} [D_{\text{KL}}(q(\mathbf{x}_K | \mathbf{x}_0) \| p(\mathbf{x}_K))]. \end{aligned}$$

\mathcal{L}_K is a constant number that can be ignored in the training, as the prior distribution $p(\mathbf{x}_K)$ is fixed:

$$p(\mathbf{x}_K) = [\bar{\beta}_K, \bar{\beta}_K, \dots, \bar{\beta}_K^*, \bar{\beta}_K^*, \dots, \bar{\gamma}_K]. \quad (7)$$

Note that $p_{\theta_1}(\mathbf{x}_{k-1}^v)$ and $p_{\theta_2}(\mathbf{x}_{k-1}^a)$ are obtained with x_0 -parameterization as follows,

$$p_{\theta_1}(\mathbf{x}_{k-1}^v | \mathbf{x}_k, \mathbf{y}, \mathbf{l}) = \sum_{\tilde{\mathbf{x}}_0^v} q(\mathbf{x}_{k-1}^v | \mathbf{x}_k, \tilde{\mathbf{x}}_0^v) p_{\theta_1}(\tilde{\mathbf{x}}_0^v | \mathbf{x}_k, \mathbf{y}, \mathbf{l}), \quad (8)$$

$$p_{\theta_2}(\mathbf{x}_{k-1}^a | \mathbf{x}_k, z_{\tilde{\mathbf{x}}_0^v}, \mathbf{l}) = \sum_{\tilde{\mathbf{x}}_0^a} q(\mathbf{x}_{k-1}^a | \mathbf{x}_k, \tilde{\mathbf{x}}_0^a) p_{\theta_2}(\tilde{\mathbf{x}}_0^a | \mathbf{x}_k, z_{\tilde{\mathbf{x}}_0^v}, \mathbf{l}) \quad (9)$$

Model Architecture. As in Eq. (8), the neural network p_{θ_1} receives \mathbf{x}_k , history \mathbf{y} , language \mathbf{l} and the diffusion timestep k as inputs. These inputs are individually embedded into embeddings h of size d via separate MLPs f , depicted as:

$$h_l = f_l(\text{CLIP}(\mathbf{l})), h_{T_i} = f_{T_i}(k), h_{x_k} = f_{x_k}(\mathbf{x}_k), h_y = f_y(\mathbf{y}),$$

where language instructions \mathbf{l} is encoded with CLIP’s language encoder (Radford et al., 2021). Afterwards, the embeddings are formulated as input tokens as $h_{\text{tokens}} = \text{LN}(h_{T_i} \times [h_l, h_{T_i}, h_{x_k}, h_y] + E^{\text{pos}})$, where E^{pos} is the positional embedding, and LN denotes layer normalization (Ba et al., 2016) for stabilizing training. The input sequence that represents a video can be extremely long so a standard Transformer with $\mathcal{O}(n^2)$ complexity is hard to fit. We adopt Perceiver Transformer (Jaegle et al., 2022) to tackle this problem, as it has been widely utilized for modeling long sequences (Shridhar et al., 2022; Goyal et al., 2023). Perceiver is a latent-space Transformer, where instead of attending to the entire input, it computes cross-attention between the input and a much smaller set of latent vectors (which are randomly initialized and trained). These latents are encoded with self-attention layers, and are cross-attended with the input to match the size for the final outputs. More details about the Perceiver Transformer are referred to §A.2.

3.3. Learning to Act via Few-Shot Fine-Tuning

During the fine-tuning stage, we leverage a limited dataset of robot data, including both videos and actions, for rapid adaptation. Both \mathbf{x}^v and \mathbf{x}^a attend to training the diffusion model. Given that p_{θ_1} has been trained sufficiently to capture fruitful information to predict future videos from history, we freeze p_{θ_1} and solely tune parameters of p_{θ_2} to minimize \mathcal{L}_{vlb} . As expressed in Eq. (9), the input of p_{θ_2} consists of \mathbf{x}_k , language \mathbf{l} , hidden representation $z_{\tilde{\mathbf{x}}_0^v}$, and

diffusion timestep k . In this case, we are tasked with predicting a sequence of action tokens x_0^a , considerably shorter than video-token sequence x_0^v , so we employ GPT2 (Radford et al., 2019) Transformer to process tokens embedded with MLPs. GPT2 has demonstrated an impressive ability to solve multi-task problems and model multimodal distributions. The model architecture of p_{θ_2} closely resembles that of MTDIFF-P (He et al., 2023).

Fast Denoising Strategy. In the denoising (inference) stage, the x_0 -parameterisation within discrete diffusion enables an expedited inference process, as discussed in (Gu et al., 2022). Concretely, rather than sampling tokens in the chain of x_K, x_{K-1}, \dots, x_0 , we can sample tokens in the chain of $x_K, x_{K-\Delta k}, \dots, x_0$ with the reverse transition:

$$p_{\theta_1}(x_{k-\Delta k}^v | x_k, \mathbf{y}, l) = \sum_{\tilde{x}_0^v} q(x_{k-\Delta k}^v | x_k, \tilde{x}_0^v) p_{\theta_1}(\tilde{x}_0^v | x_k, \mathbf{y}, l),$$

$$p_{\theta_2}(x_{k-\Delta k}^a | x_k, z_{\tilde{x}_0^v}, l) = \sum_{\tilde{x}_0^a} q(x_{k-\Delta k}^a | x_k, \tilde{x}_0^a) p_{\theta_2}(\tilde{x}_0^a | x_k, z_{\tilde{x}_0^v}, l)$$

4. Related Work

Robot Learning from Human Videos. Leveraging human videos (Goyal et al., 2017; Fang et al., 2018; Damen et al., 2021; Grauman et al., 2022) for policy learning is promising to extract commonsense knowledge from human activities, which can be shared to embodied scenarios that suffer from scarce robot data (Collaboration, 2023; Fang et al., 2023). Since the human data is actionless and the domain gap between humans and robots exists, a main branch of research employs human video to learn shareable visual representations (Burns et al., 2023; Jing et al., 2023) via time-contrastive (Ma et al., 2023b), video-language alignment (Nair et al., 2022; Karamcheti et al., 2023), value function (Bhateja et al., 2023), and perceptual skills (Huo et al., 2023; Liang et al., 2023). Visual affordance like human-object interaction hotspots (Liu et al., 2022; Goyal et al., 2022) and the post-grasp trajectory (Bahl et al., 2023) are also helpful for embodied agents in goal-conditioned imitation. Alternative methods involve extracting hand trajectories (Bahl et al., 2022; Wang et al., 2023a) or keypoints (Xiong et al., 2021) to transfer plans to robots. Different from the above methods, we eliminate the domain gaps by learning video tokens and representations for video prediction, which implicitly captures visual features, affordances, and long-term plans. Other works attempt to infer actions from videos via inverse kinematics (Bharadhwaj et al., 2023a; Ko et al., 2024), whereas we learn action prediction through policy fine-tuning without external models.

Pretraining for Generalized Policy Learning. Early works of policy adaptation emerged in meta-RL (Gupta et al., 2018; Yuan & Lu, 2022), while the pre-training and fine-tuning environments are assumed to be similar. Leveraging the transformer architecture, works perform pre-training in multi-task datasets by optimizing the multi-task policy (Lee

et al., 2022; Reed et al., 2022; Taiga et al., 2023; Thomas et al., 2023) or self-supervised objectives (Sun et al., 2023; Seo et al., 2022; Mendonca et al., 2023). In tasks involving visual observations, methods adopt visual tokens for transformer-based multi-task policy learning (Bousmalis et al., 2023; Brohan et al., 2023) and adaptation (Lin et al., 2023). Additionally, some studies pre-train a reward function through video-language correspondence (Chen et al., 2021a; Ma et al., 2023a) or diffusion models (Escontrela et al., 2023; Huang et al., 2023) for downstream RL training. Different from the previous Transformer and continuous diffusion frameworks, our work first integrates visual tokens with discrete diffusion to predict consistent videos and actions simultaneously. Concurrently, GR-1 (Wu et al., 2024) utilizes human data to pre-train a GPT-style architecture for predicting future observations. In contrast, we perform video prediction instead of step-by-step image prediction using a unified discrete diffusion architecture.

Diffusion Models for RL. Diffusion models are a powerful family of generative models (Saharia et al., 2022; Ramesh et al., 2022) that can be categorized into continuous Gaussian diffusion models and discrete diffusion models that handle discrete visual tokens or symbols (Gu et al., 2022). Continuous diffusion models have found extensive applications as multi-modal policies (Wang et al., 2023b; Pearce et al., 2023; Chi et al., 2023), environmental dynamics (Yang et al., 2024), and planners to generate action (Janner et al., 2022; Xian et al., 2023) or state sequences (Ajay et al., 2023; Chen et al., 2023), guided by desired properties. Several methods also extend the diffusion models for multi-task learning (He et al., 2023; Ni et al., 2023; Dong et al., 2024) with low-dimensional states, while we specifically address the more challenging image-based setting. UniPi (Du et al., 2023) is related to our method by performing video generation via continuous diffusion while we adopt a more flexible architecture with discrete diffusion to seamlessly connect the pre-training and fine-tuning stages, without relying on a task-specific inverse-dynamic model for acting. Additionally, we train the model on video tokens that maintain temporal consistency, while UniPi relies on super-resolution to improve the time consistency of generated frames.

5. Experiments

5.1. Benchmarks and Baselines

After the video pertaining in Ego4D (Grauman et al., 2022), we use the following robotic benchmark to learn to evaluate.

Meta-World. The Meta-World benchmark (Yu et al., 2020) contains 50 distinct manipulation tasks that require a Sawyer robot to interact with various objects with different shapes, joints, and connectivity. The action is the 3D position movements of the robot’s end effector and the gripper openness. We follow recent works (Yang et al., 2020; Sun et al., 2022)

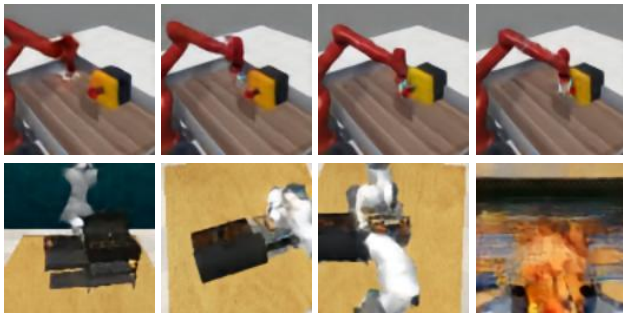


Figure 3. Single-view and multi-view images from Meta-World *button-press* and RLbench *meat-off-grill* tasks, sampled from videos predicted by p_{θ_1} .

to extend the original environment to a more challenging setting with random goals, and refer to it as MT50-rand. We train the policy with 20 demonstrations per task, and report the average success rates on 50 evaluation episodes per task.

RLBench. RLBench (James et al., 2020) is a more challenging 3D manipulation benchmark with diverse tasks concerning interactions with a wide range of objects. We select 16 tasks from RLBench to evaluate our method, where each task has several possible variations, such as the shapes, colors, sizes and positions of objects. The input observations are captured from four RGB cameras positioned at the front, left shoulder, right shoulder, and wrist. The action is an 8-dimensional vector including 3-dimensional transitions, 4-dimensional quaternion, and a binary value about gripper openness. We follow the convention by using macro steps (James & Davison, 2022), which are key turning points in the action trajectory where the gripper changes its state (open/close) or the joint velocities approach to zero. We train the policy with 10 demonstrations per task and report average success rates on 25 evaluation episodes per task.

Baselines for Meta-World. We compare the proposed method VPDD with the following baselines: (i) **R3M-Diffusion** is a discrete diffusion model sharing identical architecture with p_{θ_2} , leveraging the R3M (Nair et al., 2022) ResNet50 encoder to encode images as input. R3M is also trained on Ego4D videos and stands as the state-of-the-art (SOTA) visual representation specifically designed for manipulation tasks; (ii) **MTDIFF-P** (He et al., 2023) is the SOTA method for multi-task RL, which employs a continuous diffusion model with a Transformer architecture. Since it is designed to handle state-based input, we employ the R3M encoder to extract hidden embeddings from images, which are then fed into MTDIFF-P; (iii) **Video-MTDT** is an extension of Decision Transformer (MT) (Chen et al., 2021b), learning from multi-task data with video tokens as input; (iv) **VPDD-w/o.-human** excludes human videos during pre-training, remaining other parts unchanged. This baseline helps to ablate the effect of pre-train on large-scale human videos; (v) **SODA** (Hudson et al., 2023) is a recently proposed diffusion-based representation method that em-

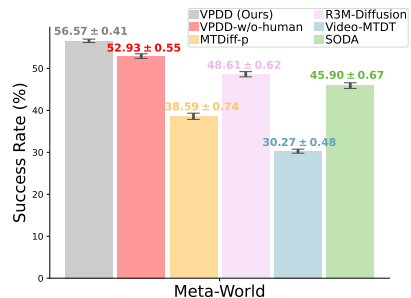


Figure 4. Average success rate across 3 seeds on MT50-rand. Each task is evaluated for 50 episodes.

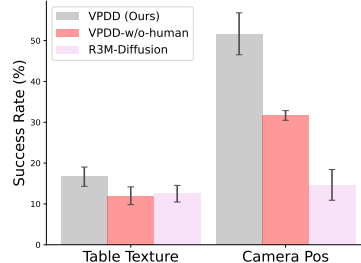


Figure 5. Average success rate across 3 seeds on *button-press-v2* and *handle-press-v2* tasks, where table texture and camera position are shifted to evaluate the generalization of different methods.

employs an encoder to generate representations z from input images to support the denoising process. We pre-train the encoder by employing the video prediction objective on the same dataset and subsequently feed the learned z into p_{θ_2} during fine-tuning. See more details in §B.

Baselines for RLBench. Learning policies for RLBench is more challenging as it requires understanding the 3D scene structure for predicting the 6D poses of end-effectors. The baselines used in Meta-World all fail in the benchmark since they are disadvantaged with single-view observations. In contrast, VPDD can predict multi-view images, implicitly recovering the 3D geometry in manipulation. Thus, we use the following SOTA imitation architectures designed for 3D manipulation: (i) **RVT** (Goyal et al., 2023) stands as the SOTA method, initially re-rendering visual observations into orthographic projections of cube views and subsequently predicting the next move based on these multi-view projections.; (ii) **PERACT** (Shridhar et al., 2022) encodes RGB-D images into voxel grid patches for 3D representation and predicts the action using the Perceiver Transformer.

5.2. Experimental Results

Question 1. Does our pre-trained diffusion model (i.e., p_{θ_1}) capable of generating high-fidelity future videos?

Although our primary contribution is not about video generation, it remains crucial to predict consistent future videos to aid in policy fine-tuning. The predicted raw videos are visually depicted in Fig. 3, with more video samples accessible at <https://video-diff.github.io>. These

Video Pre-Training via Discrete Diffusion

Method	slide block	sweep to dustpan	meat off grill	turn tap	put in drawer	close jar	drag stick	stack blocks
PERACT (10 demos) (Shridhar et al., 2022)	32	72	68	72	16	32	36	12
RVT (10 demos) (Goyal et al., 2023)	54.67 ± 1.89	76.0 ± 3.27	69.33 ± 6.80	96.0 ± 3.27	91.33 ± 6.60	22.67 ± 4.99	97.33 ± 1.89	5.33 ± 1.89
VPDD	70.67 ± 1.89	40 ± 3.27	73.33 ± 4.99	88.67 ± 3.77	24.0 ± 3.72	37.33 ± 8.22	66.67 ± 1.89	56.0 ± 5.66

Method	screw bulb	put in safe	place wine	put in cupboard	push buttons	insert peg	stack cups	place cups
PERACT (10 demos) (Shridhar et al., 2022)	28	16	20	0	56	4	0	0
RVT (10 demos) (Goyal et al., 2023)	28.0 ± 3.27	38.67 ± 4.99	45.33 ± 6.80	5.33 ± 1.89	65.33 ± 1.89	2.67 ± 1.89	2.67 ± 1.89	0 ± 0
VPDD	61.33 ± 6.80	70.67 ± 1.89	60.0 ± 6.53	30.67 ± 4.99	58.67 ± 1.89	73.33 ± 1.89	56.0 ± 5.66	30.67 ± 1.89

Table 1. Success rates (mean and std %) across 3 random seeds of various multi-task agents trained with 10 demonstrations and evaluated on 25 episodes per task. VPDD outperforms SOTA methods of RLbench, i.e., PERACT and RVT, with an average improvement of 1.24×. Note that VPDD only takes RGB images as input while both RVT and PERACT utilize additional depth images as inputs.

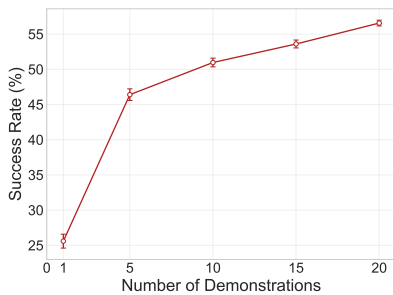


Figure 6. Average success rate across 3 seeds on MT50-rand, where VPDD is trained on a different number of demonstrations.

videos are reconstructed from predicted video tokens by using the decoder of VQ-VAE. After pre-training, the video-prediction model p_{θ_1} demonstrates the capability to generate dynamically consistent single-view videos for Meta-World and multi-view videos for RLbench. We attribute the capability of generating high-quality videos to the well-trained video codebook and the proposed discrete diffusion model learned from large-scale human data.

Question 2. *How does VPDD compare to other offline baselines for vision-based multi-task decision-making?*

To evaluate the learned policy after fine-tuning, we take the first action generated by p_{θ_2} to interact with the environment. The results on Meta-World and RLbench are referred to Fig. 4 and Table 1 respectively, yielding the following key findings: (i) VPDD outperforms other SOTA methods in success rate by a large margin. For Meta-World, VPDD performs the best across 50 tasks with random goals. For RLbench, VPDD even outperforms the SOTA imitation architectures based on voxel and multi-view representations that are carefully designed for 3D manipulation, which usually require point clouds or 3D world rendering for scene understanding. Notably, VPDD achieves a remarkable success rate on *put in cupboard*, *insert peg*, *stack cups* and *place cups*, while both RVT and PERACT struggle on these challenging tasks. This verifies the efficacy of video pre-training for few-shot policy fine-tuning; (ii) According to Fig. 4, VPDD obtains a 6.9% relative improvement through pre-training on both human and robot videos compared with VPDD-w/o.-human. Furthermore, VPDD surpasses R3M with a notable 16.4% higher success rate, demonstrating the potential of our diffusion representation via video pre-

training; (iii) R3M-Diffusion outperforms MTDIFF-P which employ R3M encoder with continuous diffusion architecture by 26.0%, and Video-MTDT with Transformer architecture by 60.6%. This highlights the superior capacity of discrete diffusion models compared to other approaches.

Question 3. *How does VPDD generalize to unseen scenes?*

Following Xie et al. (2023), we alter the camera position and table texture in the visual scene of Meta-World to assess the generalization ability of our method. According to Fig. 5, VPDD exhibits superior generalizability, attributed to the training of the diffusion representation on large-scale diverse human videos. Regarding the shift in camera position, VPDD outperforms the *VPDD-w/o.-human* by 63% and R3M by 252%. Detailed settings can be found in §C.3.

Question 4. *Can VPDD maintain satisfactory performance when provided with fewer robotic demonstrations?*

Leveraging the large-scale video pre-training, VPDD can learn the policy using only a small number of demonstrations. To validate the sample efficiency of our method, we conduct an ablation study on the number of demonstrations used in the fine-tuning stage. The results, depicted in Fig. 6, reveal that the performance of VPDD exhibits linear growth after training on 5 or more demonstrations, indicating the potential for VPDD to achieve better performance with increased demonstration data. Moreover, VPDD maintains a comparable success rate even when only 1 demonstration is used in the fine-tuning process.

Question 5. *Does VPDD outperforms other diffusion-based representation learning method?*

To verify the representation capability inherent in our unified discrete diffusion framework, we reproduce SODA (Hudson et al., 2023), which serves as a strong diffusion representation method. As shown in Fig. 4, VPDD outperforms SODA in the context of policy fine-tuning. We hypothesize that VPDD provides coarse-to-fine representations (i.e., $z_{\tilde{x}_0^y}$) throughout the action-denoising steps from $K \rightarrow 1$, exactly encapsulating useful information the denoising network focuses on at each step (Ho et al., 2020). In contrast, SODA produces representation z that remains constant across all steps during action denoising.

6. Conclusion

We propose VPDD, a video-based policy learning framework via discrete diffusion. With a VQ-VAE tokenizer, we bridge the gap between human and robot videos by a discrete latent codebook. We leverage a unified discrete diffusion for pre-training on large-scale actionless mixture videos and subsequent fine-tuning the policy on a limited number of robot demonstrations. Experiments demonstrate that VPDD achieves superior performance on a variety of challenging manipulation tasks and showcases impressive generalization ability benefited from human video prediction. Discussions of limitations and future works are given in §D.

Broader Impact

This paper presents work whose goal is to advance the field of Machine Learning. There are many potential societal consequences of our work, none of which we feel must be specifically highlighted here.

References

- Ajay, A., Du, Y., Gupta, A., Tenenbaum, J. B., Jaakkola, T. S., and Agrawal, P. Is conditional generative modeling all you need for decision making? In *International Conference on Learning Representations*, 2023.
- Austin, J., Johnson, D. D., Ho, J., Tarlow, D., and van den Berg, R. Structured denoising diffusion models in discrete state-spaces, 2023.
- Ba, L. J., Kiros, J. R., and Hinton, G. E. Layer normalization. *CoRR*, abs/1607.06450, 2016. URL <http://arxiv.org/abs/1607.06450>.
- Bahl, S., Gupta, A., and Pathak, D. Human-to-robot imitation in the wild. 2022.
- Bahl, S., Mendonca, R., Chen, L., Jain, U., and Pathak, D. Affordances from human videos as a versatile representation for robotics. In *Proceedings of the IEEE/CVF Conference on Computer Vision and Pattern Recognition*, pp. 13778–13790, 2023.
- Bharadhwaj, H., Gupta, A., Tulsiani, S., and Kumar, V. Zero-shot robot manipulation from passive human videos. *arXiv preprint arXiv:2302.02011*, 2023a.
- Bharadhwaj, H., Vakil, J., Sharma, M., Gupta, A., Tulsiani, S., and Kumar, V. Roboagent: Generalization and efficiency in robot manipulation via semantic augmentations and action chunking. In *First Workshop on Out-of-Distribution Generalization in Robotics at CoRL 2023*, 2023b.
- Bhateja, C., Guo, D., Ghosh, D., Singh, A., Tomar, M., Vuong, Q., Chebotar, Y., Levine, S., and Kumar, A. Robotic offline RL from internet videos via value-function pre-training. In *NeurIPS 2023 Foundation Models for Decision Making Workshop*, 2023.
- Blattmann, A., Dockhorn, T., Kulal, S., Mendelevitch, D., Kilian, M., Lorenz, D., Levi, Y., English, Z., Voleti, V., Letts, A., et al. Stable video diffusion: Scaling latent video diffusion models to large datasets. *arXiv preprint arXiv:2311.15127*, 2023.
- Bousmalis, K., Vezzani, G., Rao, D., Devin, C., Lee, A. X., Bauza, M., Davchev, T., Zhou, Y., Gupta, A., Raju, A., et al. Robocat: A self-improving foundation agent for robotic manipulation. *arXiv preprint arXiv:2306.11706*, 2023.
- Brohan, A., Brown, N., Carbajal, J., Chebotar, Y., Dabis, J., Finn, C., Gopalakrishnan, K., Hausman, K., Herzog, A., and et al. Rt-1: Robotics transformer for real-world control at scale. In *Robotics: Science and Systems*, 2023.
- Burns, K., Witzel, Z., Hamid, J. I., Yu, T., Finn, C., and Hausman, K. What makes pre-trained visual representations successful for robust manipulation? *arXiv preprint arXiv:2312.12444*, 2023.
- Chen, A. S., Nair, S., and Finn, C. Learning generalizable robotic reward functions from ”in-the-wild” human videos. *arXiv preprint arXiv:2103.16817*, 2021a.
- Chen, H., Lu, C., Ying, C., Su, H., and Zhu, J. Offline reinforcement learning via high-fidelity generative behavior modeling. In *International Conference on Learning Representations*, 2023.
- Chen, L., Lu, K., Rajeswaran, A., Lee, K., Grover, A., Laskin, M., Abbeel, P., Srinivas, A., and Mordatch, I. Decision transformer: Reinforcement learning via sequence modeling. *Advances in neural information processing systems*, 34:15084–15097, 2021b.
- Chi, C., Feng, S., Du, Y., Xu, Z., Cousineau, E., Burchfiel, B., and Song, S. Diffusion policy: Visuomotor policy learning via action diffusion. *arXiv preprint arXiv:2303.04137*, 2023.
- Collaboration, O. X. Open x-embodiment: Robotic learning datasets and RT-X models. *CoRR*, abs/2310.08864, 2023.
- Damen, D., Doughty, H., Farinella, G. M., Fidler, S., Furnari, A., Kazakos, E., Moltisanti, D., Munro, J., Perrett, T., Price, W., and Wray, M. The epic-kitchens dataset: Collection, challenges and baselines. *IEEE Transactions on Pattern Analysis and Machine Intelligence (TPAMI)*, 43(11):4125–4141, 2021. doi: 10.1109/TPAMI.2020.2991965.

- Dong, Z., Yuan, Y., Hao, J., Ni, F., Mu, Y., Zheng, Y., Hu, Y., Lv, T., Fan, C., and Hu, Z. Aligndiff: Aligning diverse human preferences via behavior-customisable diffusion model. In *International Conference on Learning Representations*, 2024.
- Du, Y., Yang, S., Dai, B., Dai, H., Nachum, O., Tenenbaum, J. B., Schuurmans, D., and Abbeel, P. Learning universal policies via text-guided video generation. In *Neural Information Processing Systems*, 2023.
- Escontrela, A., Adeniji, A., Yan, W., Jain, A., Peng, X. B., Goldberg, K., Lee, Y., Hafner, D., and Abbeel, P. Video prediction models as rewards for reinforcement learning. In *Neural Information Processing Systems*, 2023.
- Fang, H.-S., Fang, H., Tang, Z., Liu, J., Wang, C., Wang, J., Zhu, H., and Lu, C. Rh20t: A comprehensive robotic dataset for learning diverse skills in one-shot. *Towards Generalist Robots: Learning Paradigms for Scalable Skill Acquisition@ CoRL2023*, 3:5, 2023.
- Fang, K., Wu, T.-L., Yang, D., Savarese, S., and Lim, J. J. Demo2vec: Reasoning object affordances from online videos. In *IEEE Conference on Computer Vision and Pattern Recognition*, pp. 2139–2147, 2018.
- Goyal, A., Xu, J., Guo, Y., Blukis, V., Chao, Y.-W., and Fox, D. RVT: Robotic view transformer for 3d object manipulation. In *7th Annual Conference on Robot Learning*, 2023.
- Goyal, M., Modi, S., Goyal, R., and Gupta, S. Human hands as probes for interactive object understanding. In *Proceedings of the IEEE/CVF Conference on Computer Vision and Pattern Recognition*, pp. 3293–3303, 2022.
- Goyal, R., Ebrahimi Kahou, S., Michalski, V., Materzynska, J., Westphal, S., Kim, H., Haenel, V., Fruend, I., Yianilos, P., Mueller-Freitag, M., et al. The” something something” video database for learning and evaluating visual common sense. In *Proceedings of the IEEE international conference on computer vision*, pp. 5842–5850, 2017.
- Grauman, K., Westbury, A., Byrne, E., Chavis, Z., Furnari, A., Girdhar, R., Hamburger, J., Jiang, H., Liu, M., Liu, X., et al. Ego4d: Around the world in 3,000 hours of egocentric video. In *IEEE/CVF Conference on Computer Vision and Pattern Recognition*, pp. 18995–19012, 2022.
- Grauman, K., Westbury, A., Torresani, L., Kitani, K., Malik, J., Afouras, T., Ashutosh, K., Baiyya, V., Bansal, S., Boote, B., et al. Ego-exo4d: Understanding skilled human activity from first-and third-person perspectives. *arXiv preprint arXiv:2311.18259*, 2023.
- Gu, S., Chen, D., Bao, J., Wen, F., Zhang, B., Chen, D., Yuan, L., and Guo, B. Vector quantized diffusion model for text-to-image synthesis. In *IEEE/CVF Conference on Computer Vision and Pattern Recognition*, pp. 10696–10706, 2022.
- Gupta, A., Mendonca, R., Liu, Y., Abbeel, P., and Levine, S. Meta-reinforcement learning of structured exploration strategies. *Advances in neural information processing systems*, 31, 2018.
- Hafner, D., Lillicrap, T., Ba, J., and Norouzi, M. Dream to control: Learning behaviors by latent imagination. In *International Conference on Learning Representations*, 2020.
- Hafner, D., Lillicrap, T. P., Norouzi, M., and Ba, J. Mastering atari with discrete world models. In *International Conference on Learning Representations*, 2021.
- Hansen, N. A., Su, H., and Wang, X. Temporal difference learning for model predictive control. In *International Conference on Machine Learning*, pp. 8387–8406. PMLR, 2022.
- He, H., Bai, C., Xu, K., Yang, Z., Zhang, W., Wang, D., Zhao, B., and Li, X. Diffusion model is an effective planner and data synthesizer for multi-task reinforcement learning. In *Neural Information Processing Systems*, 2023.
- Ho, J., Jain, A., and Abbeel, P. Denoising diffusion probabilistic models. *Advances in neural information processing systems*, 33:6840–6851, 2020.
- Hoogeboom, E., Nielsen, D., Jaini, P., Forré, P., and Welling, M. Argmax flows and multinomial diffusion: Learning categorical distributions. In *Advances in Neural Information Processing Systems*, 2021.
- Hu, M., Zheng, C., Yang, Z., Cham, T.-J., Zheng, H., Wang, C., Tao, D., and Suganthan, P. N. Unified discrete diffusion for simultaneous vision-language generation. In *International Conference on Learning Representations*, 2023.
- Huang, T., Jiang, G., Ze, Y., and Xu, H. Diffusion reward: Learning rewards via conditional video diffusion. *arXiv preprint arXiv:2312.14134*, 2023.
- Hudson, D. A., Zoran, D., Malinowski, M., Lampinen, A. K., Jaegle, A., McClelland, J. L., Matthey, L., Hill, F., and Lerchner, A. Soda: Bottleneck diffusion models for representation learning. *arXiv preprint arXiv:2311.17901*, 2023.
- Huo, M., Ding, M., Xu, C., Tian, T., Zhu, X., Mu, Y., Sun, L., Tomizuka, M., and Zhan, W. Human-oriented representation learning for robotic manipulation, 2023.

- Jaegle, A., Borgeaud, S., Alayrac, J.-B., Doersch, C., Ionescu, C., Ding, D., Koppula, S., Zoran, D., Brock, A., Shelhamer, E., Henaff, O. J., Botvinick, M., Zisserman, A., Vinyals, O., and Carreira, J. Perceiver IO: A general architecture for structured inputs & outputs. In *International Conference on Learning Representations*, 2022.
- James, S. and Davison, A. J. Q-attention: Enabling efficient learning for vision-based robotic manipulation. *IEEE Robotics and Automation Letters*, 7(2):1612–1619, 2022.
- James, S., Ma, Z., Arrojo, D. R., and Davison, A. J. Rlbench: The robot learning benchmark & learning environment. *IEEE Robotics and Automation Letters*, 5(2):3019–3026, 2020.
- James, S., Wada, K., Laidlow, T., and Davison, A. J. Coarse-to-fine q-attention: Efficient learning for visual robotic manipulation via discretisation. In *Proceedings of the IEEE/CVF Conference on Computer Vision and Pattern Recognition*, pp. 13739–13748, 2022.
- Janner, M., Li, Q., and Levine, S. Offline reinforcement learning as one big sequence modeling problem. *Advances in neural information processing systems*, 34: 1273–1286, 2021.
- Janner, M., Du, Y., Tenenbaum, J. B., and Levine, S. Planning with diffusion for flexible behavior synthesis. In *International Conference on Machine Learning*, 2022.
- Jing, Y., Zhu, X., Liu, X., Sima, Q., Yang, T., Feng, Y., and Kong, T. Exploring visual pre-training for robot manipulation: Datasets, models and methods. In *2023 IEEE/RSJ International Conference on Intelligent Robots and Systems (IROS)*, pp. 11390–11395. IEEE, 2023.
- Karamcheti, S., Nair, S., Chen, A. S., Kollar, T., Finn, C., Sadigh, D., and Liang, P. Language-driven representation learning for robotics. In *Robotics: Science and Systems (RSS)*, 2023.
- Kingma, D. P. and Ba, J. Adam: A method for stochastic optimization. *arXiv preprint arXiv:1412.6980*, 2014.
- Ko, P.-C., Mao, J., Du, Y., Sun, S.-H., and Tenenbaum, J. B. Learning to act from actionless videos through dense correspondences. In *International Conference on Learning Representations*, 2024.
- Lee, K.-H., Nachum, O., Yang, M. S., Lee, L., Freeman, D., Guadarrama, S., Fischer, I., Xu, W., Jang, E., Michalewski, H., et al. Multi-game decision transformers. *Advances in Neural Information Processing Systems*, 35: 27921–27936, 2022.
- Liang, Z., Mu, Y., Ma, H., Tomizuka, M., Ding, M., and Luo, P. Skilldiffuser: Interpretable hierarchical planning via skill abstractions in diffusion-based task execution. *arXiv preprint arXiv:2312.11598*, 2023.
- Lin, X., So, J., Mahalingam, S., Liu, F., and Abbeel, P. Spawnnet: Learning generalizable visuomotor skills from pre-trained networks, 2023.
- Liu, S., Tripathi, S., Majumdar, S., and Wang, X. Joint hand motion and interaction hotspots prediction from egocentric videos. In *Proceedings of the IEEE/CVF Conference on Computer Vision and Pattern Recognition*, pp. 3282–3292, 2022.
- Lu, J., Batra, D., Parikh, D., and Lee, S. Vilbert: Pre-training task-agnostic visiolinguistic representations for vision-and-language tasks. *Advances in neural information processing systems*, 32, 2019.
- Ma, Y. J., Kumar, V., Zhang, A., Bastani, O., and Jayaraman, D. LIV: Language-image representations and rewards for robotic control. In *International Conference on Machine Learning*, volume 202, pp. 23301–23320, 2023a.
- Ma, Y. J., Sodhani, S., Jayaraman, D., Bastani, O., Kumar, V., and Zhang, A. VIP: Towards universal visual reward and representation via value-implicit pre-training. In *International Conference on Learning Representations*, 2023b.
- Mendonca, R., Bahl, S., and Pathak, D. Structured world models from human videos. 2023.
- Mu, Y., Zhang, Q., Hu, M., Wang, W., Ding, M., Jin, J., Wang, B., Dai, J., Qiao, Y., and Luo, P. EmbodiedGPT: Vision-language pre-training via embodied chain of thought. In *Neural Information Processing Systems*, 2023.
- Nair, S., Rajeswaran, A., Kumar, V., Finn, C., and Gupta, A. R3m: A universal visual representation for robot manipulation. In *6th Annual Conference on Robot Learning*, 2022.
- Ni, F., Hao, J., Mu, Y., Yuan, Y., Zheng, Y., Wang, B., and Liang, Z. Metadiffuser: Diffusion model as conditional planner for offline meta-rl. 2023.
- OpenAI et al. Gpt-4 technical report, 2023.
- Pearce, T., Rashid, T., Kanervisto, A., Bignell, D., Sun, M., Georgescu, R., Macua, S. V., Tan, S. Z., Momennejad, I., Hofmann, K., and Devlin, S. Imitating human behaviour with diffusion models. In *International Conference on Learning Representations*, 2023.

- Penedo, G., Malartic, Q., Hesslow, D., Cojocaru, R., Cappelli, A., Alobeidli, H., Pannier, B., Almazrouei, E., and Launay, J. The refinedweb dataset for falcon llm: outperforming curated corpora with web data, and web data only. *arXiv preprint arXiv:2306.01116*, 2023.
- Radford, A., Wu, J., Child, R., Luan, D., Amodei, D., and Sutskever, I. Language models are unsupervised multitask learners. 2019.
- Radford, A., Kim, J. W., Hallacy, C., Ramesh, A., Goh, G., Agarwal, S., Sastry, G., Askell, A., Mishkin, P., Clark, J., Krueger, G., and Sutskever, I. Learning transferable visual models from natural language supervision, 2021.
- Radosavovic, I., Xiao, T., James, S., Abbeel, P., Malik, J., and Darrell, T. Real-world robot learning with masked visual pre-training. *CoRL*, 2022.
- Ramesh, A., Dhariwal, P., Nichol, A., Chu, C., and Chen, M. Hierarchical text-conditional image generation with clip latents. *arXiv preprint arXiv:2204.06125*, 1(2):3, 2022.
- Reed, S., Zolna, K., Parisotto, E., Colmenarejo, S. G., Novikov, A., Barth-Maron, G., Gimenez, M., Sulsky, Y., Kay, J., Springenberg, J. T., et al. A generalist agent. *arXiv preprint arXiv:2205.06175*, 2022.
- Russakovsky, O., Deng, J., Su, H., Krause, J., Satheesh, S., Ma, S., Huang, Z., Karpathy, A., Khosla, A., Bernstein, M. S., Berg, A. C., and Fei-Fei, L. Imagenet large scale visual recognition challenge. *International Journal of Computer Vision*, 115:211 – 252, 2014.
- Saharia, C., Chan, W., Saxena, S., Li, L., Whang, J., Denton, E., Ghasemipour, S. K. S., Ayan, B. K., Mahdavi, S. S., Lopes, R. G., Salimans, T., Ho, J., Fleet, D. J., and Norouzi, M. Photorealistic text-to-image diffusion models with deep language understanding, 2022.
- Seo, Y., Lee, K., James, S. L., and Abbeel, P. Reinforcement learning with action-free pre-training from videos. In *International Conference on Machine Learning*, pp. 19561–19579. PMLR, 2022.
- Shaw, K., Bahl, S., and Pathak, D. Videodex: Learning dexterity from internet videos. In *6th Annual Conference on Robot Learning*, 2022. URL <https://openreview.net/forum?id=qUhkhHw8Dz>.
- Shridhar, M., Manuelli, L., and Fox, D. Perceiver-actor: A multi-task transformer for robotic manipulation. In *6th Annual Conference on Robot Learning*, 2022.
- Sohl-Dickstein, J., Weiss, E. A., Maheswaranathan, N., and Ganguli, S. Deep unsupervised learning using nonequilibrium thermodynamics, 2015.
- Sun, L., Zhang, H., Xu, W., and Tomizuka, M. Paco: Parameter-compositional multi-task reinforcement learning. In Oh, A. H., Agarwal, A., Belgrave, D., and Cho, K. (eds.), *Advances in Neural Information Processing Systems*, 2022.
- Sun, Y., Ma, S., Madaan, R., Bonatti, R., Huang, F., and Kapoor, A. SMART: Self-supervised multi-task pretraining with control transformers. In *International Conference on Learning Representations*, 2023.
- Taiga, A. A., Agarwal, R., Farebrother, J., Courville, A., and Bellemare, M. G. Investigating multi-task pretraining and generalization in reinforcement learning. In *International Conference on Learning Representations*, 2023.
- Thomas, G., Cheng, C.-A., Loynd, R., Frujeri, F. V., Vineet, V., Jalobeanu, M., and Kolobov, A. Plex: Making the most of the available data for robotic manipulation pretraining. In *Conference on Robot Learning*, pp. 2624–2641. PMLR, 2023.
- Touvron, H., Lavril, T., Izacard, G., Martinet, X., Lachaux, M.-A., Lacroix, T., Rozière, B., Goyal, N., Hambro, E., Azhar, F., et al. Llama: Open and efficient foundation language models. *arXiv preprint arXiv:2302.13971*, 2023a.
- Touvron, H., Martin, L., Stone, K., Albert, P., Almahairi, A., Babaei, Y., Bashlykov, N., Batra, S., Bhargava, P., Bhosale, S., et al. Llama 2: Open foundation and fine-tuned chat models. *arXiv preprint arXiv:2307.09288*, 2023b.
- van den Oord, A., Vinyals, O., and Kavukcuoglu, K. Neural discrete representation learning. In *Advances in Neural Information Processing Systems*, volume 30. Curran Associates, Inc., 2017.
- Vaswani, A., Shazeer, N., Parmar, N., Uszkoreit, J., Jones, L., Gomez, A. N., Kaiser, Ł., and Polosukhin, I. Attention is all you need. *Advances in neural information processing systems*, 30, 2017.
- Walke, H. R., Black, K., Zhao, T. Z., Vuong, Q., Zheng, C., Hansen-Estruch, P., He, A. W., Myers, V., Kim, M. J., Du, M., Lee, A., Fang, K., Finn, C., and Levine, S. Bridgedata v2: A dataset for robot learning at scale. In *Conference on Robot Learning*, pp. 1723–1736, 2023a.
- Walke, H. R., Black, K., Zhao, T. Z., Vuong, Q., Zheng, C., Hansen-Estruch, P., He, A. W., Myers, V., Kim, M. J., Du, M., et al. Bridgedata v2: A dataset for robot learning at scale. In *Conference on Robot Learning*, pp. 1723–1736. PMLR, 2023b.
- Wang, C., Fan, L., Sun, J., Zhang, R., Fei-Fei, L., Xu, D., Zhu, Y., and Anandkumar, A. Mimicplay: Long-horizon imitation learning by watching human play. *arXiv preprint arXiv:2302.12422*, 2023a.

- Wang, Z., Hunt, J. J., and Zhou, M. Diffusion policies as an expressive policy class for offline reinforcement learning. In *International Conference on Learning Representations*, 2023b.
- Wu, H., Jing, Y., Cheang, C., Chen, G., Xu, J., Li, X., Liu, M., Li, H., and Kong, T. Unleashing large-scale video generative pre-training for visual robot manipulation. In *International Conference on Learning Representations*, 2024.
- Wu, J., Ma, H., Deng, C., and Long, M. Pre-training contextualized world models with in-the-wild videos for reinforcement learning. In *Thirty-seventh Conference on Neural Information Processing Systems*, 2023. URL <https://openreview.net/forum?id=8GuEVzAUQS>.
- Xian, Z., Gkanatsios, N., Gervet, T., Ke, T.-W., and Fragkiadaki, K. Chaineddiffuser: Unifying trajectory diffusion and keypose prediction for robotic manipulation. In *7th Annual Conference on Robot Learning*, 2023.
- Xiao, T., Radosavovic, I., Darrell, T., and Malik, J. Masked visual pre-training for motor control. *arXiv:2203.06173*, 2022.
- Xie, A., Lee, L., Xiao, T., and Finn, C. Decomposing the generalization gap in imitation learning for visual robotic manipulation. *arXiv preprint arXiv:2307.03659*, 2023.
- Xiong, H., Li, Q., Chen, Y.-C., Bharadhwaj, H., Sinha, S., and Garg, A. Learning by watching: Physical imitation of manipulation skills from human videos. In *2021 IEEE/RSJ International Conference on Intelligent Robots and Systems (IROS)*, pp. 7827–7834. IEEE, 2021.
- Yan, W., Zhang, Y., Abbeel, P., and Srinivas, A. Videogpt: Video generation using vq-vae and transformers, 2021.
- Yang, M., Du, Y., Ghasemipour, K., Tompson, J., Schuurmans, D., and Abbeel, P. Learning interactive real-world simulators. In *International Conference on Learning Representations*, 2024.
- Yang, R., Xu, H., Wu, Y., and Wang, X. Multi-task reinforcement learning with soft modularization. *Advances in Neural Information Processing Systems*, 33:4767–4777, 2020.
- Yu, T., Quillen, D., He, Z., Julian, R., Hausman, K., Finn, C., and Levine, S. Meta-world: A benchmark and evaluation for multi-task and meta reinforcement learning. In *Conference on robot learning*, pp. 1094–1100. PMLR, 2020.
- Yuan, H. and Lu, Z. Robust task representations for offline meta-reinforcement learning via contrastive learning. In *International Conference on Machine Learning*, pp. 25747–25759. PMLR, 2022.
- Zhang, H., Xu, W., and Yu, H. Generative planning for temporally coordinated exploration in reinforcement learning. In *International Conference on Learning Representations*, 2022.

A. The Details of VPDD

A.1. Discrete Diffusion

Discrete diffusion models with a mask-and-replace strategy generate sequences from [MASK] tokens. In this paper, they are trained by sampling a sequence $\mathbf{x}_0 = [\mathbf{x}^v, \mathbf{x}^a]$, masking tokens according to a linear schedule in Gu et al. (2022) that corresponds to increasing the probability of being in the absorbing state linearly over time, and learning to predict the masked tokens given language l and historical videos. Specifically, for the proposed unified transition matrix \mathbf{Q}_k in Eq. (6), the computation of diffusion process $q(\mathbf{x}_k|\mathbf{x}_0)$ in Eq. (4) can also be obtained in the following closed-form (Hu et al., 2023):

$$\begin{aligned} \overline{\mathbf{Q}}_k \mathbf{x}_0 &= \overline{\alpha}_k \mathbf{x}_0 + \left[\overline{\gamma}_k - \mathbb{1}(x_0) \overline{\beta}_k - \mathbb{1}^*(x_0) \overline{\beta}_k^* \right] \mathbf{x}_{[M]} + \mathbb{1}(x_0) \overline{\beta}_k + \mathbb{1}^*(x_0) \overline{\beta}_k^*, \\ \text{where } \mathbb{1}(x_0) &= \begin{cases} 1 & \text{if } \operatorname{argmax} x_0 \in [0, J), \\ 0 & \text{otherwise.} \end{cases}, \quad \mathbb{1}^*(x_0) = \begin{cases} 1 & \text{if } \operatorname{argmax} x_0 \in [J, J + J^*), \\ 0 & \text{otherwise.} \end{cases}, \end{aligned} \quad (10)$$

$\mathbf{x}_{[M]} = \mathbf{x} \leftarrow \operatorname{argmax} x = J + J^*$ and $\overline{\alpha}_k, \overline{\beta}_k, \overline{\beta}_k^*, \overline{\gamma}_k$ are the corresponding cumulative product.

The reverse process predicts $\tilde{\mathbf{x}}_0^v$ and $\tilde{\mathbf{x}}_0^a$ by training denoising network $p_{\theta_1}(\tilde{\mathbf{x}}_0^v|\mathbf{x}_k, \mathbf{y}, \mathbf{l})$ and $p_{\theta_2}(\tilde{\mathbf{x}}_0^a|\mathbf{x}_k, z_{\tilde{\mathbf{x}}_0^v}, \mathbf{l})$, respectively. Then the forward process is used to compute $p_{\theta_1}(\mathbf{x}_{k-1}^v|\mathbf{x}_k, \mathbf{y}, \mathbf{l})$ as expressed in Eq. (8) and $p_{\theta_2}(\mathbf{x}_{k-1}^a|\mathbf{x}_k, z_{\tilde{\mathbf{x}}_0^v}, \mathbf{l})$ as expressed in Eq. (9).

A.2. Perceiver Transformer

We use the Perceiver Transformer (Jaegle et al., 2022) to encode extremely long input sequences, which improves the computation efficiency. We maintain a set of latent vectors z_Q of dimensions $\mathbb{R}^{2048 \times 256}$ which are randomly initialized. Then we compute cross attention between the input sequence and z_Q . The process is illustrated in Fig. 7. z_Q are processed with 6 self-attention layers, and then decoded into output with the same dimension space of input via cross attention.

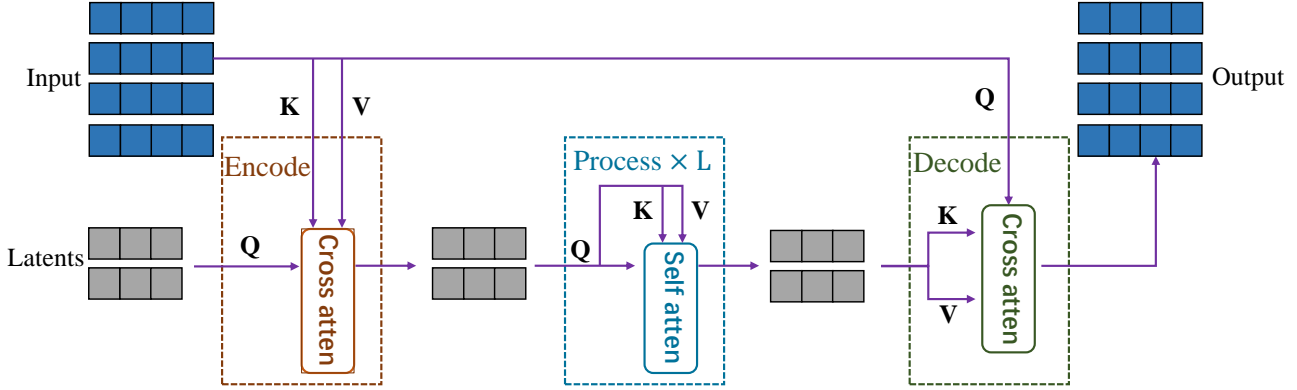


Figure 7. Illustration of Perceiver Transformer architecture. Perceiver is a latent-space transformer. Q, K, V represent queries, keys, and values, respectively. We use $L = 6$ self attention layers in our implementation.

A.3. Implementation Details

In this section, we give the pseudocodes of pre-training and fine-tuning in Alg. 1 and Alg. 2 respectively. Then we describe the details of the training process, architecture and hyperparameters:

- Following Hoogeboom et al. (2021), we sample diffusion timestep $k \sim q(k)$ with a importance sampling strategy, where $q(k) \propto \sqrt{\mathbb{E}[\mathcal{L}_{v|b}^2]}$.
- We set batch size as 20 for pre-training and 40 for fine-tuning. We train our model using Adam optimizer (Kingma & Ba, 2014) with $2e^{-4}$ learning rate for $2e^6$ training steps.
- For pre-training, we represent our denoising network p_{θ_1} as a Perceiver Transformer described in §A.2. MLP f_t , which processes the language embeddings given by the CLIP encoder, MLP f_y , which processes the historical video tokens, and

MLP $f_{\mathbf{x}_k}$ are 2-layered MLPs (preended by a layer norm (Ba et al., 2016) and with Mish activation). MLP f_{T_i} , which processes diffusion timestep k , is a 2-layered MLP (preended by a Sinusoidal embedding and with Mish activation). Finally, we use a linear layer to project the encodings given by the Perceiver Transformer into the original dimension space of the input.

- For fine-tuning, we represent our denoising network p_{θ_2} as a GPT2 Transformer. Similar to the architecture of p_{θ_1} , we first use MLPs with Mish activation to project different inputs into the same hidden dimension space, and then recover the encodings given by the GPT2 Transformer into the original dimension space via a linear layer.
- We choose the sequence length $H = 4$ and $M = 1$ for future actions and videos prediction.
- We set $h = 20$ which means that we predict future videos after 20 steps.
- We set diffusion timesteps $K = 100$.

B. The Details of Baselines

We describe the implementation details of baselines used in our experiments as follows:

- **R3M-Diffusion.** We borrow the pre-trained R3M encoder from <https://github.com/facebookresearch/r3m>, and leverage the encoder to encode sing-view RGB images in Meta-World and multi-view RGB images in RL Bench. Thus, we skip the pre-training process and directly train our discrete diffusion model on the robot data. The model architecture and hyper-parameters of R3M-Diffusion are almost the same as p_{θ_2} . The encoded hidden representation encoded by R3M is denoted as z_{R3M} , then the denoising network can be written as $p_{\theta}(\mathbf{x}_{k-1}^a | \mathbf{x}_k, z_{R3M}, \mathbf{l})$.
- **MTDIFF-P.** We borrow the official codes of MTDIFF-P from <https://github.com/tinnerhrhe/MTDiff>. In order to process high-dimensional images instead of low-dimensional states, we leverage the R3M encoder in R3M-Diffusion to obtain the visual representations.
- **VIDEO-MTDT.** We use the language l to indicate tasks, which are encoded as a vector with size 2048 by the same CLIP encoder used in VPDD. We take the video tokens used in VPDD as the states. Then we follow the implementation from <https://github.com/kz1/decision-transformer/> to train Video-MTDT on the limited robot data.
- **VPDD-w/o-human.** During the pre-training stage of VPDD, we remove the human videos and only use the robot videos for training.
- **SODA.** Following the SODA paper (Hudson et al., 2023) and open-sourced codes from <https://github.com/FutureXiang/soda>, we first maintain an encoder E_{SODA} equipped with the same Perceiver Transformer in p_{θ_1} . Then during the pre-training stage, a representation z is first encoded by E_{SODA} conditioning on e_t and l , i.e., $z = E_{\text{SODA}}(e_t, l)$. Then \mathbf{x}_{k-1} is obtained via the following process:

$$\begin{aligned} \mathbf{x}_{k-1} &= \text{Attn}(\mathbf{x}_k, z) \\ \mathbf{x}_{k-1} &= \text{Attn}(\mathbf{x}_{k-1}, \mathbf{x}_{k-1}), \end{aligned} \tag{11}$$

where Attn is an attention operation (Vaswani et al., 2017; Lu et al., 2019) where the queries are formed from x , the keys and values from y . The encoder is trained end-to-end and to minimize the same loss term \mathcal{L}_{vlb} . During the fine-tuning stage, $z_{\tilde{\mathbf{x}}_0}$ is replaced of z output by E_{SODA} . The model architecture and other hyper-parameters during fine-tuning remain the same.

Algorithm 1 Pre-Training Stage of VPDD

Initialize: given unified transition matrix $\{Q_k\}$, well-trained VQVAE, training iterations N , initial network parameters θ_1 and θ_2 , learning rate η .

- 1: **for** video clips v_t in $\{\tau_i\}$ **do**
 - 2: $e_t \leftarrow \text{VQVAE-Encoder}(v_t)$
 - 3: **end for**
 - 4: **for** $n = 1$ **to** N **do**
 - 5: Sample a batch $\mathcal{B} = (\mathbf{x}^v, \mathbf{x}^a, \mathbf{y}, \mathbf{l})$ from human and robot videos, where $\mathbf{x}^a \leftarrow \phi$
 - 6: Sample diffusion timestep k from $[1, K]$ with importance sampling strategy
 - 7: $\mathbf{x}_k \leftarrow q(\mathbf{x}_k | \mathbf{x}_0)$, where $\mathbf{x}_0 = [\mathbf{x}^v, \mathbf{x}^a]$ \triangleright Eq. (10) and (4)
 - 8: $\mathcal{L}_{\text{vib}} = \begin{cases} \mathcal{L}_0 & \text{if } k = 1, \\ \mathcal{L}_{k-1} & \text{otherwise.} \end{cases}$ \triangleright Eq. (6)
 - 9: $\theta_1 \leftarrow \theta_1 - \eta \nabla_{\theta_1} \mathcal{L}$ \triangleright Adam optimizer
 - 10: **end for**
-

Algorithm 2 Fine-Tuning Stage of VPDD and Evaluation

Fine-Tuning Process

Initialize: given unified transition matrix $\{Q_k\}$, well-trained VQVAE, training iterations N , pre-trained network parameters θ_1 and initial parameters θ_2 , learning rate η .

- 1: **for** video clips v_t and actions a_t in $\{\tau_i\}$ **do**
- 2: $e_t \leftarrow \text{VQVAE-Encoder}(v_t)$, $a_t \leftarrow \text{Discretize}(a_t)$
- 3: **end for**
- 4: **for** $n = 1$ **to** N **do**
- 5: Sample a batch $\mathcal{B} = (\mathbf{x}^v, \mathbf{x}^a, \mathbf{y}, \mathbf{l})$ from videos and discretized actions dataset.
- 6: Sample diffusion timestep k from $[1, K]$ with a importance sampling strategy
- 7: $\mathbf{x}_k \leftarrow q(\mathbf{x}_k | \mathbf{x}_0)$, where $\mathbf{x}_0 = [\mathbf{x}^v, \mathbf{x}^a]$ \triangleright Eq. (10) and (4)
- 8: $\mathcal{L}_{\text{vib}} = \begin{cases} \mathcal{L}_0 & \text{if } k = 1, \\ \mathcal{L}_{k-1} & \text{otherwise.} \end{cases}$ \triangleright Eq. (6)
- 9: $\theta_2 \leftarrow \theta_2 - \eta \nabla_{\theta_2} \mathcal{L}$ \triangleright Adam optimizer
- 10: **end for**

Evaluation Process

- 1: Given a task, reset the environment
 - 2: Obtain the initial video clips v_0 , language instructions \mathbf{l}
 - 3: **for** $t = 0$ **to** t_{\max} **do**
 - 4: Initialize $[\mathbf{x}_K^v, \mathbf{x}_K^a] \sim p(\mathbf{x}_K)$ \triangleright Eq. (7)
 - 5: Construct $\mathbf{y} \leftarrow e_t = \text{VQVAE-Encoder}(v_t)$
 - 6: **for** $k = K$ **to** 1 **do**
 - 7: Sample $\mathbf{x}_{k-1}^v \sim p_{\theta_1}(\mathbf{x}_{k-1}^v | \mathbf{x}_k, \mathbf{y}, \mathbf{l})$ and obtain $z_{\tilde{\mathbf{x}}_0^v}$ from p_{θ_1} encoding \triangleright Eq. (8)
 - 8: Sample $\mathbf{x}_{k-1}^a \sim p_{\theta_2}(\mathbf{x}_{k-1}^a | \mathbf{x}_k, z_{\tilde{\mathbf{x}}_0^v}, \mathbf{l})$ \triangleright Eq. (9)
 - 9: $\mathbf{x}_{k-1} = [\mathbf{x}_{k-1}^v, \mathbf{x}_{k-1}^a]$
 - 10: **end for**
 - 11: Obtain predicted videos via VQVAE-Decoder(\mathbf{x}_0^v)
 - 12: Reconstruct executable action sequence $[a_t, \dots, a_{t+H-1}]$ from \mathbf{x}_0^a
 - 13: Execute the first action a_t as the current action to interact with the environment
 - 14: Obtain the next observed image(s), and update v_t
 - 15: **end for**
-

C. Datasets and Experiments

C.1. Dataset

Meta-World. We use the official codes from <https://github.com/Farama-Foundation/Metaworld> to collect 20 expert demonstrations for each task in Meta-World. The image size is 260×260 . The dimension of action is 4, representing the 3D position movements of the end effector and the variation of gripper openness. Every demonstration collected has 150 time steps.

RLBench. We use the official codes from <https://github.com/peract/peract> to generate a dataset for RLBench via a motion planner. Each demonstration consists of multi-view RGB images (i.e., front, left shoulder, right shoulder and wrist) and 8-dimensional actions including 3-dimensional transitions, 4-dimensional quaternion and a binary value about gripper openness. Following prior works (James & Davison, 2022; Shridhar et al., 2022), we extract macro actions (keyframe actions) from collected demonstrations and leverage networks to predict the keyframe actions instead of consistent continuous actions. Specifically, a set of keyframe actions $\{k_1, k_2, \dots, k_m\} \subset \mathcal{A}$ is captured with a simple heuristic: an action is a keyframe if (1) the joint velocities are near zero and (2) the gripper open state has not changed. Each data point in the demonstration τ can then be cast as a “predict the next (best) keyframe action” task (James et al., 2022). In this way, the sequence length of actions that need to be predicted is significantly reduced from hundreds of small steps to typically less than 10 macro steps.

C.2. Task Details

Task	Variation Type	# of Variations	Language Template
slide block	color	4	“slide the block to <u> </u> target”
sweep to dustpan	size	2	“sweep dirt to the <u> </u> dustpan”
meat off grill	category	2	“take the <u> </u> off the grill”
turn tap	placement	2	“turn <u> </u> tap”
put in drawer	placement	3	“put the item in the <u> </u> drawer”
close jar	color	20	“close the <u> </u> jar”
drag stick	color	20	“use the stick to drag the cube onto the <u> </u> target”
stack blocks	color, count	60	“stack <u> </u> <u> </u> blocks”
screw bulb	color	20	“screw in the <u> </u> light bulb”
put in safe	placement	3	“put the money away in the safe on the <u> </u> shelf”
place wine	placement	3	“stack the wine bottle to the <u> </u> of the rack”
put in cupboard	category	9	“put the <u> </u> in the cupboard”
push buttons	color	50	“push the <u> </u> button, [then the <u> </u> button]”
insert peg	color	20	“put the ring on the <u> </u> spoke”
stack cups	color	20	“stack the other cups on top of the <u> </u> cup”
place cups	count	3	“place <u> </u> cups on the cup holder”

Table 2. Language-Conditioned Tasks in RLBench (James et al., 2020) with various variations.

We take Meta-World as a main benchmark to evaluate our method and baselines, which consists of 50 diverse manipulation tasks. The poses and positions of goals are randomly generated during evaluation. These tasks require an agent to identify the observed sing-view RGB images and reach the goals with the correct behavior. See Fig. 8 for a sample visualization of the tasks.

We select 16 tasks out of 100 tasks from RLBench (James et al., 2020) that involve at least two or more variations to evaluate the multi-task and generalization capabilities of agents. Task variations include randomly sampled colors, sizes, counts, placements, and categories of objects. The set of colors include 20 instances: $\text{colors} = \{\text{red, maroon, lime, green, blue, navy, yellow, cyan, magenta, silver, gray, orange, olive, purple, teal, azure, violet, rose, black, white}\}$. The set of sizes include 2 instances: $\text{sizes} = \{\text{short, tall}\}$. The set of counts include 3 instances: $\text{counts} = \{1, 2, 3\}$. The placements and object categories are specific to each task. For instance, `put in cupboard` includes 9 YCB objects. In addition to these semantic variations, objects are placed on the tabletop at random poses. The

tasks in RLBench require an agent to process multi-view RGB images properly and generalize to different variations that could be unseen in training. The details of variations for each task are referred to Table 2.

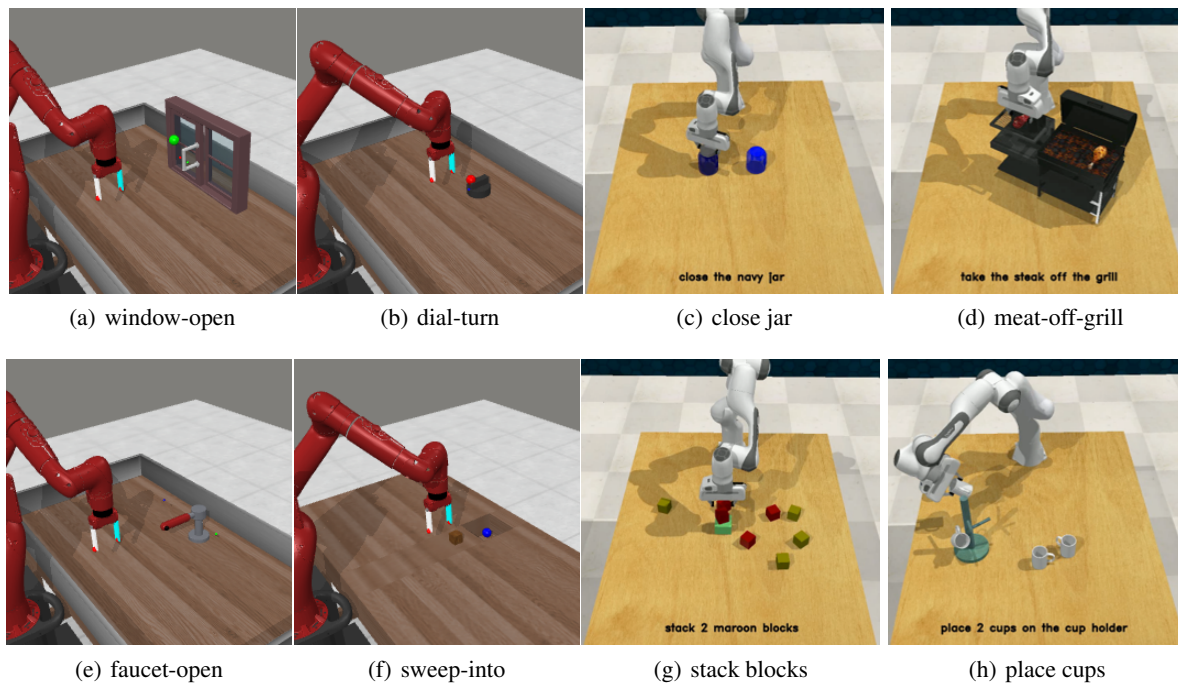


Figure 8. Visualization of several tasks in Meta-World and RLBench.

C.3. Experimental Setup

To evaluate the generalization ability of our method, we change the camera position and table texture in the Meta-World benchmark to generate out-of-distribution observations. Following Xie et al. (2023) and using the official codes from <https://github.com/RLAgent/factor-world>, we set the camera at another corner position and generate unseen table texture randomly while rendering. See Fig. 9 for visualization.

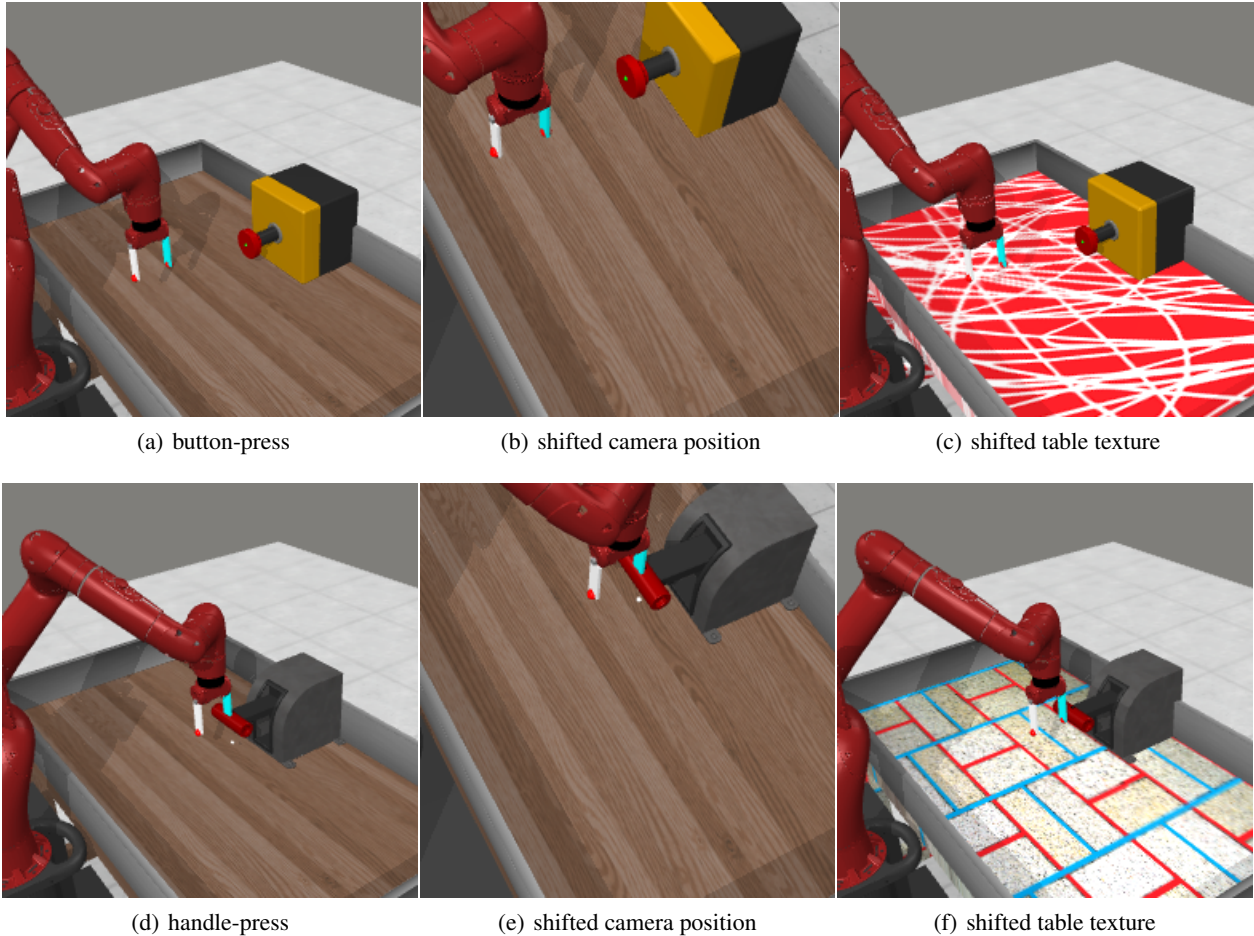


Figure 9. A visualized example of shifted camera position and table texture on *button-press-v2* and *handle-press-v2* tasks. Table texture is generated randomly during evaluation.

D. Limitations and Future Work

We present illustrative samples of robot videos generated using discrete diffusion model p_{θ_1} in Fig. 3 and Fig. 10. More samples are available at <https://video-diff.github.io>. It is noteworthy that VPDD is able to generate dynamic consistent future videos, incorporating information beneficial for low-level control while maintaining coherence across distinct perspectives. However, it is imperative to acknowledge that our primary contribution is not on generating high-quality videos with exceptional resolution and meticulous semantic details. Consequently, some blurriness may be observed in our predicted videos, exemplified by deviations in the gripper’s pose. See Fig. 11 for a failure example.

For future work, we could consider enhancing the coherence of videos across diverse views by leveraging the recently released Ego-exo4d data (Grauman et al., 2023). This extension encompasses considerations beyond solely temporal dynamics. Moreover, for the augmentation of video quality and the optimization of decision-making performance, it is worth exploring to scale up both the training dataset and model capacity.

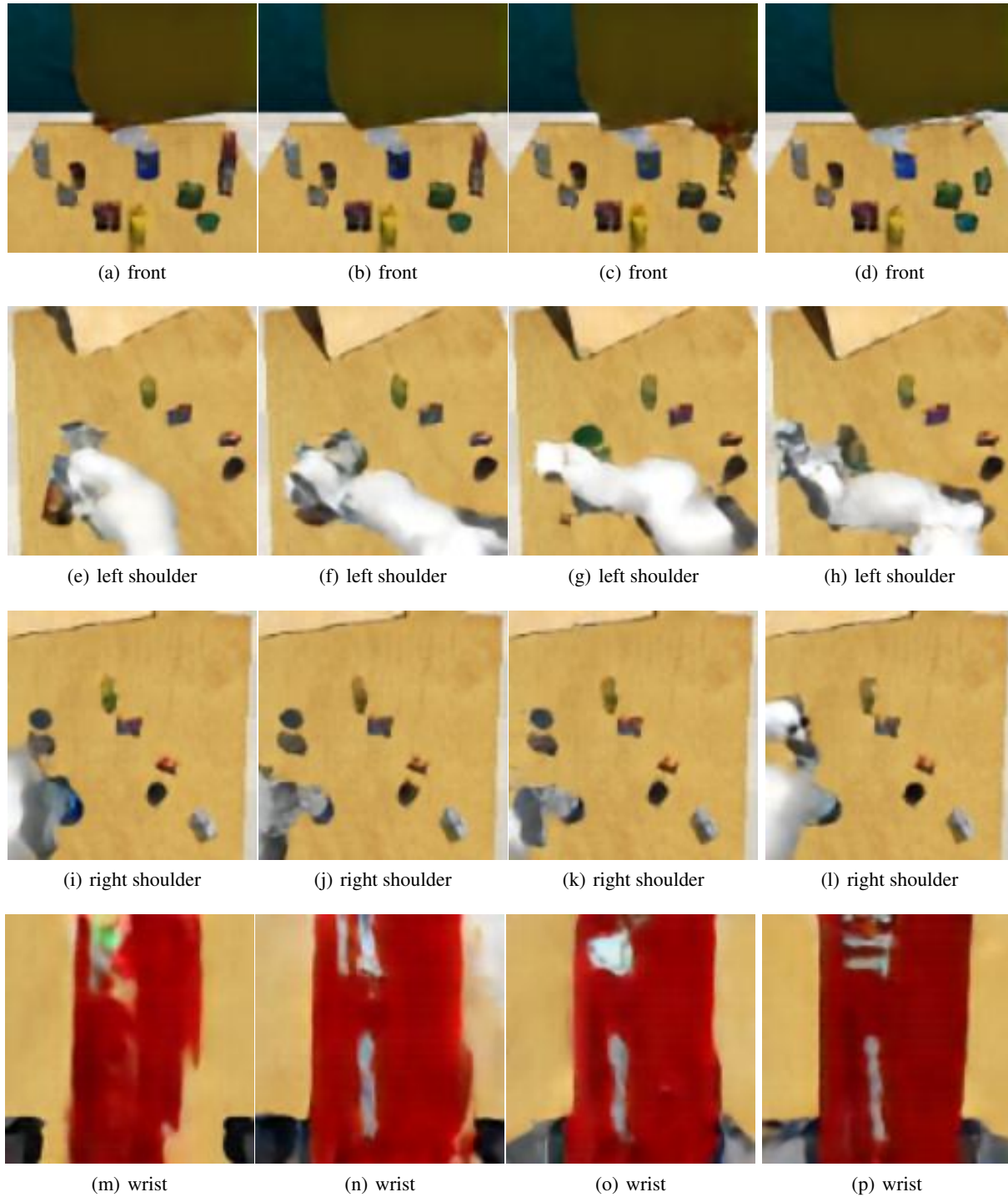


Figure 10. Predicted video given by p_{θ_1} for task *put the crackers in the cupboard*.

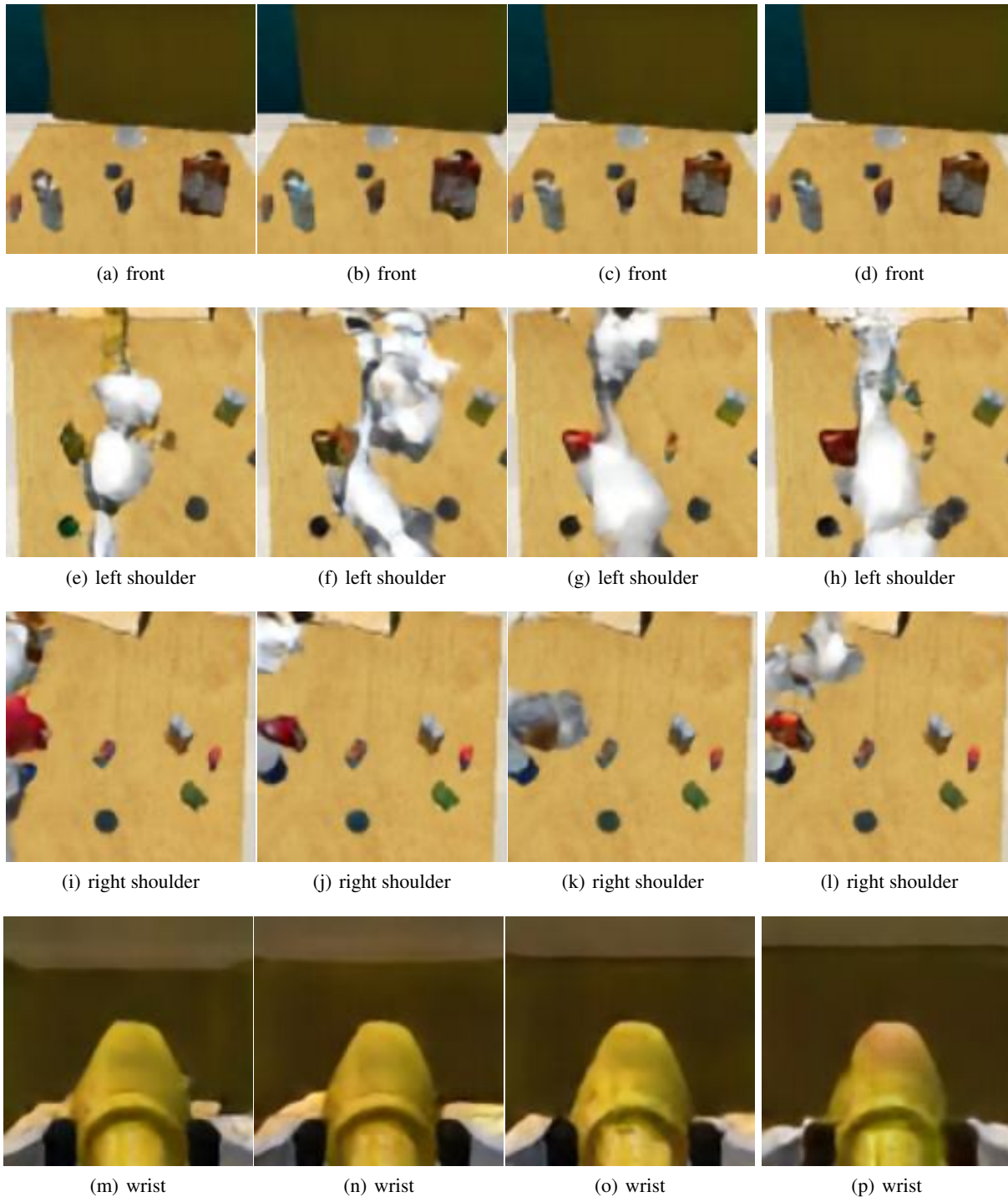


Figure 11. Predicted video given by p_{θ_1} for task *put the mustard in the cupboard*. The pose of the robotic arm in the video is somewhat blurry, with deficiencies in correspondence across different views.